INVESTIGATION OF POSSIBLE PERTURBATION OF GAMMA-GAMMA DIRECTIONAL CORRELATIONS

A THESIS

Presented to

The Faculty of the Graduate Division

by

Mustafa Rauf Sarper

In Partial Fulfillment

of the Requirements for the Degree

Doctor of Philosophy

in the School of Physics

Georgia Institute of Technology

June, 1973

INVESTIGATION OF POSSIBLE PERTURBATION

OF GAMMA-GAMMA DIRECTIONAL CORRELATIONS

Approved:

Chairman

Date approved by Chairman: July 26, 1973

ACKNOWLEDGMENTS

The author wishes to express his sincere gratitude to his research Professors, Drs. L. D. Wyly and C. H. Braden for suggesting the thesis topic as well as their continous guidance, encouragement and help, during this research project.

The author is deeply thankful to the members of the nuclear group who have contributed a great deal to this project. He wishes to acknowledge the assistance of Dr. E. T. Patronis, Jr, and Professor N. S. Kendrick who constructed and maintained part of the experimental apparatus. He also wishes to thank Mr. J. T. Callahan for constructing the electromagnet and his assistance in maintaining various components, Dr. J. B. Salzberg for his computer programs which facilitated rapid data analysis, Dr. D. A. McClure for making his equipment available throughout this project.

The author is thankful to Dr. C. W. Gorton for his kind considerations and acknowledges the assistance of Dr. M. E. McLain, Jr., and Mr. R. C. McFarland in preparing the sources.

Finally, the author thanks his loving wife for her invaluable help in editing and typing this manuscript as well as for sharing the physical and emotional burden of these years.

TABLE OF CONTENTS

TABLE OF CONTENTS (Concluded)

LIST OF TABLES

LIST OF FIGURES

LIST OF FIGURES (Concluded)

SUMMARY

The theory of perturbed directional correlations predicts the possible attenuation of the gamma-gamma directional correlation coefficients in the event the half-life of the intermediate state is longer than about 10^{-11} second. If such perturbations are due to static magnetic interactions between the nuclear magnetic moment of a nucleus and the surrounding electron shell, such coupling can be broken up by applying a strong, static magnetic field parallel to the direction of one of the observed gamma rays.

Magnetic decoupling experiments were performed to investigate the possibility of attenuation of the gamma-gamma directional correlations in the decays of Sb^{125}, Sm^{153}, and Ce^{143}. The 427-35.5 keV cascade in Sb^{125}, which proceeds through a 1.6 nanosecond intermediate level, the 70-103 keV cascade in Sm^{153}, which proceeds through a 3.8 nanosecond level, and the 293-57 keV cascade in Ce^{143}, which proceeds through a 4.2 nanosecond level, suggest the possibility of such attenuation.

An electromagnet which furnished fields up to 7800 gauss was constructed to carry out these experiments. An on-line PDP-8 digital computer, which facilitated a high degree of automation, was used to collect, reduce and analyze data.

The preliminary investigations were directed towards checking the experimental apparatus and comparing results with those of Stiening and Deutsch. These preliminary experiments involved the 1270-123 keV

cascade in Eu^{154}. A fixed 3 X 3 inch NaI(Tl) crystal and a 25 cc Ge(Li) detector were utilized in conjunction with a fast-slow coincidence arrangement which had a resolving time of 33 nanoseconds. The single channel pulse height analyzer window in the NaI detector was set to include the 1270 keV gamma peak and the coincidence spectrum of the 123 keV gamma ray was observed in the Ge(Li) detector. Data were collected at 90°, 180° and 270° positions only, due to physical limitations imposed by the electromagnet. The results of these experiments showed a definite magnetic decoupling effect as the external magnetic field parallel to 1270 keV gamma ray was increased to 6000 gauss from its initial value of 60 gauss. The second order directional correlation coefficient, A_2, was measured to be 0.21, 0.23, and 0.24 at 60, 500 and 6000 gauss, respectively. Stiening and Deutsch have reported A_2 values of 0.18 and 0.21 at 0 and 3200 gauss, respectively.

Next, the 427-35.5 keV cascade in Sb^{125} was investigated using a similar experimental arrangement with the exception of replacing the Ge(Li) detector with a Si(Li) detector. The NaI single channel analyzer window was set to include the 427 keV peak and the coincidence spectrum of the 35.5 keV gamma ray and the 27 keV Te X-rays was observed in the Si(Li) detector. The X-ray coincidence spectrum was expected to be isotropic and it was found to be so. Heavy lead shielding was utilized in order to minimize the effects of scattering and cross-talk. The second order directional correlation coefficient A_2 was observed to be 0.19 both at 0.4 and at 6000 gauss. These results indicate that there is no static magnetic coupling between the magnetic moment of the nucleus and the electron cloud.

The 70-103 keV cascade in Sm^{153} was investigated using two 25 cc Ge(Li) detectors where the stationary detector was set to include the portion of the spectrum near the 103 keV peak and the movable detector was set on the 70 keV peak. The outputs of these detectors went through similar fast-slow coincidence arrangements. Heavy lead and magnetic shieldings were used as before to reduce scattering effects as well as the effect of the magnetic fields on the movable detector.

Two sets of experiments were conducted here. The first set comprised magnetic decoupling experiments performed at field strengths of 0 and 6000 gauss. No attenuation was found and the A_2 coefficient for this cascade was isotropic within the experimental error. To confirm this, the magnet was taken off and further directional correlation experiments were performed. These results also indicated that the A_2 coefficient for the 70-103 keV cascade is isotropic within the experimental error of $\pm$ 0.03.

The 293-57 keV cascade in Ce^{143} was investigated using the stationary 3 X 3 inch NaI(Tl) detector and a 25 cc Ge(Li) detector. The single channel analyzer of the NaI detector was set to include the region around the 293 keV photopeak and the single channel analyzer of the Ge(Li) detector was set to accept the 57 keV photopeak. The corresponding outputs were channeled into the fast-slow coincidence circuitry as in the other experiments. The NaI detector was shielded from the effects of the magnetic fields.

Magnetic decoupling experiments were performed utilizing magnetic field strengths of 0, 3000, 5000, 6200 and 7800 gauss. The second order directional correlation coefficient, A_2, was measured to be 0.18

at 7800 gauss. A decoupling effect was observed in comparing this result with the A_2 value of 0.11 obtained at zero field.

CHAPTER I

INTRODUCTION

One of the important problems of low energy nuclear physics is the determination of the properties of nuclear energy levels. A nuclear state can be characterized by its energy, total angular momentum, parity, magnetic moment, electric quadrupole moment, partial level widths and total transition probability. An effective tool of nuclear spectroscopy for the determination of angular momenta and parities of excited states is the study of the angular correlations and the directional polarization correlations of successive nuclear radiations emitted from these states.

Unperturbed Angular Correlations

The theory of angular correlations in nuclear radiations was first introduced by Hamilton (1). Basically, the theory of angular correlations (2, 3) concerns itself with the decay of a nucleus from a first level A by emitting a radiation R_1 into the intermediate state B and then through the emission of a second radiation R_2 into the final state C (see Figure 1). If we choose the directions of these two radiations to be $\vec{R}_1$ and $\vec{R}_2$, respectively, and further restrict the direction $\vec{R}_1$ to be fixed, then the relative probability $W(\theta)\, d\Omega$ that the radiation R_2 is emitted at an angle θ with respect to the direction $\vec{R}_1$ of the radiation R_1 into the solid angle $d\Omega$ is called the angular correlation function.

This angular correlation function depends on the electric and

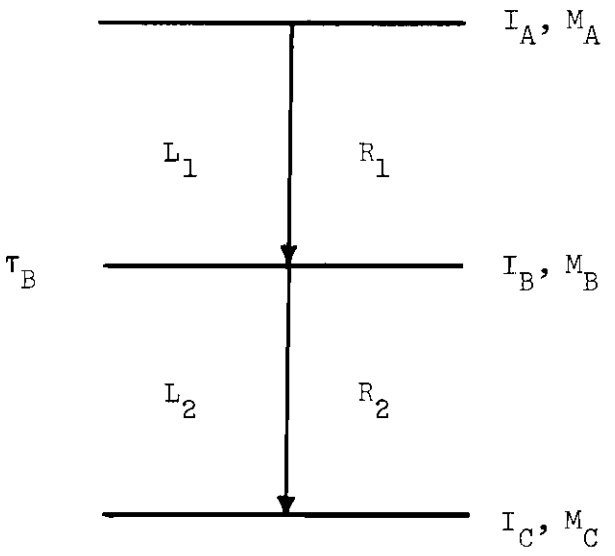

Figure 1. A Cascade Involving Two Radiations R_1 and R_2

magnetic multipole nature of the radiations R_1 and R_2 as well as upon the properties of the three levels A, B and C. The intensity distribution of one radiation alone is isotropic in space due to the random orientation of the nuclear spin of the emitting nuclear levels. However, anisotropic radiation can arise when certain orientations of the nuclear angular momentum are preferred with respect to some axis. In the first step of the above cascade the radiation from a single transition $A \rightarrow B$ with equally populated magnetic sublevels M_A is always isotropic. On the other hand, if one observes the first radiation R_1 in a given direction $\vec{R}_1$ then the sublevels M_B of the intermediate state B will be populated depending on the different transition probabilities $M_A \rightarrow M_B$. Then the second radiation R_2 which corresponds to the sum of all $M_B \rightarrow M_C$ transitions will in general have a definite anisotropic distribution with respect to the direction $\vec{R}_1$. This anisotropic radiation distribution of the second radiation with respect to the first radiation is known as the angular correlation of the two nuclear radiations.

The angular correlation function can be written as (4, 5, 6)

$$W(\theta) = \sum_{k=0}^{k_{max}} A_k P_k (\cos\theta) \qquad (1)$$

where the P_k's are the Legendre polynomials of k^{th} order and the A_k's are the angular correlation coefficients. The k indices must be even integers such that $(4)\ k_{max} \leq \min(2I_B, 2L_1, 2L_2)$ where I_B is the angular momentum of the intermediate level and L_1 and L_2 are the angular momenta of the first and second radiations, respectively.

The coefficients A_k depend upon the dynamic and static properties

of the A, B and C levels (4). Furthermore, these A_k coefficients can be split into two factors where the first factor involves the transition $A \rightarrow B$ and the second factor the transition $B \rightarrow C$. These A_k coefficients have been calculated by Biedenharn and Rose (7) for many types of transitions, where

$$A_k = A_k^{(1)} (A \rightarrow B) \times A_k^{(2)} (B \rightarrow C). \qquad (2)$$

In the expression for $W(\theta)$, A_0 is usually chosen to be unity for normalization purposes. Only even k values are used in equation (1) due to the fact that the polarizations of the radiations R_1 and R_2 are not measured. If the polarizations of these radiations are to be included, then the summation must include odd k values.

Once the theory has been established, an experiment can be set up to check the theory. The experiment includes two detectors D_1 and D_2 which detect the two radiations R_1 and R_2, respectively (see Figure 2). By the employment of suitable coincidence circuitry with a short resolving time (10^{-8} second to 10^{-6} second) one can distinguish the two radiations which are genetically related, i.e. R_1 and R_2 that come from the same nucleus, from accidental coincidences due to radiations emitted by two nuclei. The dependence of the coincidence rate on the angle θ, after certain corrections have been made for the accidental coincidences and the finite solid angle of the detectors, gives a measure of the angular correlation. The first successful angular correlation experiments were performed by Brady and Deutsch (8).

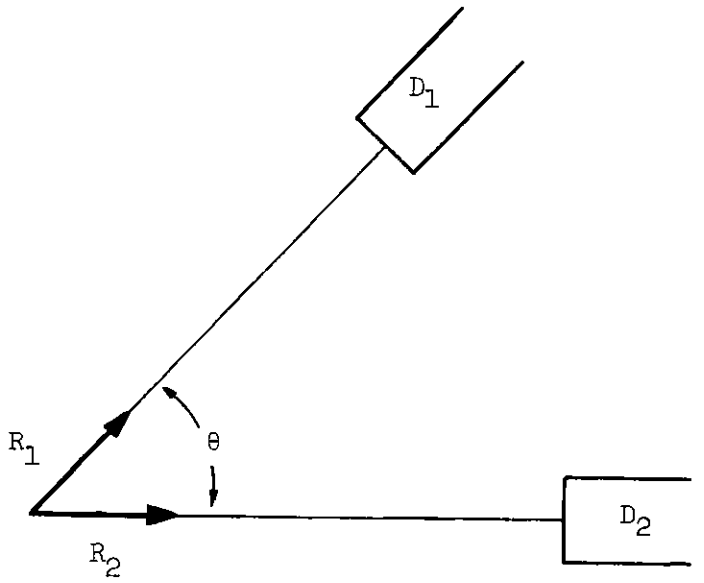

Figure 2. Experimental Arrangement of Counters

Perturbed Angular Correlations

The pioneer investigations of gamma-gamma correlations by Hamilton (1) were made with the restriction that torques due to extra-nuclear fields be small enough to have a negligible effect on the angular correlations. In most experiments, however, it is very difficult to decide whether the measured correlation function is undisturbed or not. The undisturbed angular correlation is observed if there is no change in the magnetic sublevel population during the lifetime of the intermediate state. If the lifetime of the intermediate nuclear state is longer than about 10^{-11} second, there exists the possibility that the magnetic and electric fields of the surroundings partially or completely destroy the angular correlation. In general, for a free atom which is in a S_0 state, no interaction is expected to take place between the nucleus and the electron shell. However, a nucleus is normally in either a liquid or a solid environment where the atom is not a free atom in a S_0 state. Also, due to the preceding nuclear transitions, the electron shell may not remain in its ground state during the gamma emission. Therefore, the observation of perturbed angular correlations might be expected in many instances.

The perturbed correlation function will be dependent on the physical and chemical state of the source as well as on the delay time between the two channels of the coincidence circuit which detects the incoming radiations R_1 and R_2. It is possible to study the attenuation of the angular correlation function by four different types of experiments:

(a) One can change the delay time between the two channels for

a given source and observe the effect on the angular correlation.

(b) The delay time can be kept constant and the physical state of the source can be altered.

(c) One can keep the delay time constant and apply a magnetic field which is perpendicular to the direction of the two gamma rays.

(d) In some cases it may be possible to break up the perturbation and thus restore the unperturbed correlation function.

Experiments of type (a) are difficult to apply where the lifetime of the intermediate level is about 1 nanosecond. Experiments of type (b) can be performed under special circumstances but it is difficult to establish the unperturbed correlation. In experiments of type (c), the measurement of the rotation angle of the angular correlation pattern allows one to determine the g-factor (9) of the intermediate state. An experiment of type (d) is considered most appropriate to the case of interest to us and is discussed in the following sections, with additional details included in Appendix A.

The theory of angular correlations has been extended by Goertzel (10) to take into account the effect of the perturbations on the intermediate state. Alder (11) extended the theory to apply to various experimental situations. Abragam and Pound (12) have treated magnetic dipole and electric quadrupole interactions as well as the effects of time-dependent fields. The static interactions can be described by the semiclassical vector model and the following discussions will be along these lines.

Static Magnetic Fields

Static fields can be either magnetic or electric in nature. From

the classical point of view, the magnetic moment $\bar{\mu}_B$ of a nucleus precesses about the direction in which the magnetic field is applied (Figure 3). The magnetic moment $\bar{\mu}_B$ in this figure is actually the time average value of the sum of spin and orbital magnetic moments. The projections of I_B along the direction of the field, the Z-direction, are limited by the quantization property to discrete values which lie between I_B and $-I_B$. The energy levels which were degenerate before the application of the external field are now separated. If the direction of emission of one radiation is chosen to coincide with the axis of quantization (Z-axis) then the populations of the M_B levels will not be altered. This means that the projections of the I_B on the axis of quantization do not change as the nuclear moment of the intermediate state precesses around the axis of quantization. Thus, one can obtain the unperturbed correlation function by the application of a sufficiently strong static magnetic field, along the direction of one radiation, which breaks up the coupling between the nuclear magnetic moment $\bar{\mu}_B$ and the electron shell.

In the case of a weak applied magnetic field $\bar{B}_0$, the resultant angular momentum $\bar{P}$, which is the vector sum of the nuclear angular momentum $\bar{I}_B$ and the electron shell angular momentum $\bar{J}$, precesses around the direction of the applied field (Figure 4). Since the electron shell magnetic moment $\bar{\mu}_J$ is usually about three orders of magnitude larger than the nuclear magnetic moment $\bar{\mu}_B$, we expect the interaction between the magnetic field and the electron shell magnetic moment to be dominant.

For larger values of $\bar{B}_0$ the interaction energy between $\bar{B}_0$ and $\bar{\mu}_J$ becomes much larger than the interaction energy between $\bar{\mu}_B$ and $\bar{\mu}_J$.

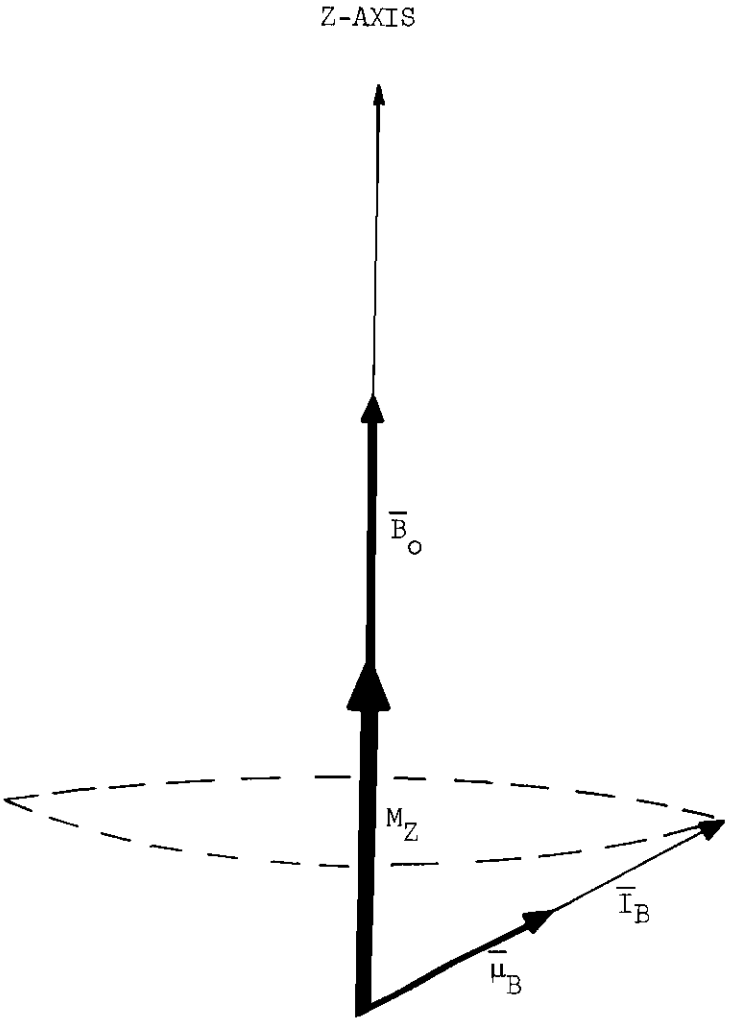

Figure 3. Precession of Angular Momentum and Magnetic Moment about a Magnetic Field

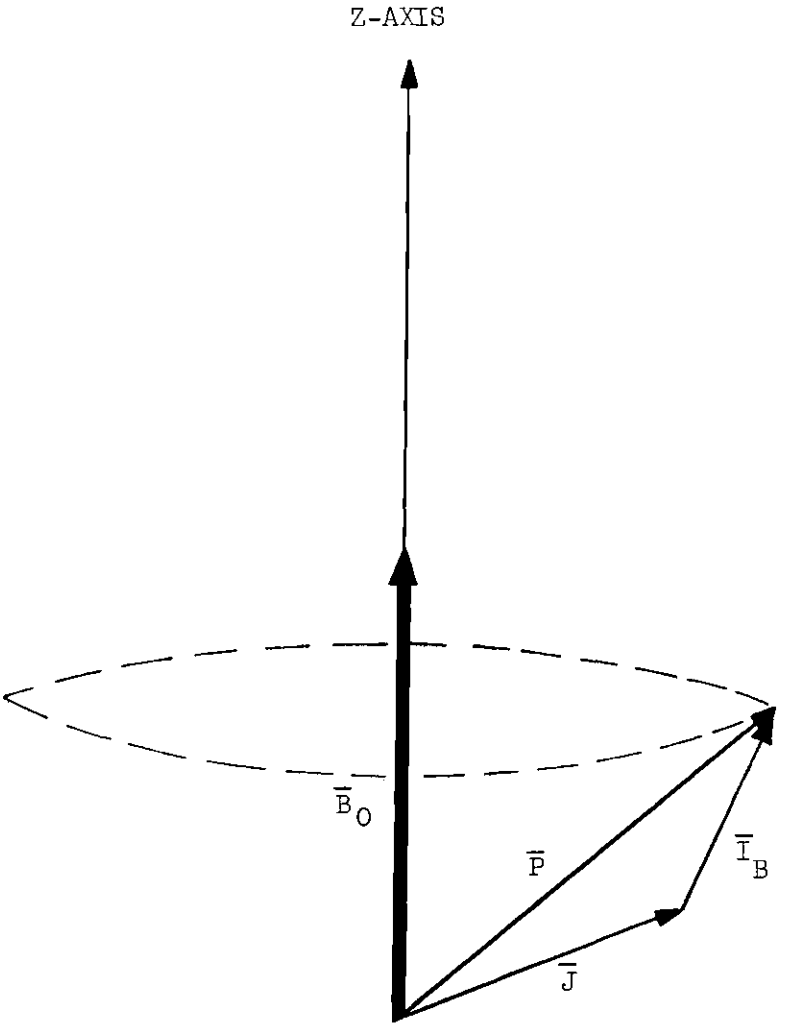

Figure 4. The Case of a Weak Applied Magnetic Field. (The resultant angular momentum $\bar{P}$, which is the vector sum of the nuclear angular momentum $\bar{I}_B$ and the electron shell angular momentum $\bar{J}$, precesses around the applied field $\bar{B}_0$.)

This strong interaction breaks the coupling between the nucleus and the electron shell. The result of this decoupling is shown in Figure 5 where the nuclear angular momentum $\bar{I}_B$ and the electron shell angular momentum $\bar{J}$ precess independently about the field axis. In the case of such decoupling, if the strong external magnetic field $\bar{B}_0$ is applied in the direction of emission of one of the nuclear radiations, one will observe the unperturbed angular correlation. The criterion for decoupling can be given by

$$B_0 \mu_J \gg h\Delta\nu$$

where $h\Delta\nu$ is the energy of the hyperfine splitting. An external field of a few thousand gauss is expected to be sufficient to accomplish the decoupling in most cases for liquid sources (9).

In the general case of the static field, the axis of quantization may not coincide with the axis of the magnetic field. Then the population of the M_B states along the axis of quantization will be changing periodically whereas the population of the M_B states along the field axis will remain the same. Since the population of the M_B states along the quantization axis determines the angular distribution of the second radiation, we expect the angular correlation to be altered. In general we do not expect a complete washing out of the angular correlation due to the fact that the M_B states along the direction of quantization will not be equally populated. As a result a "hard core"(5) value for the angular correlation remains. By applying a field (5), (13) perpendicular to the plane containing both radiations, it is possible to completely wash out the angular correlation.

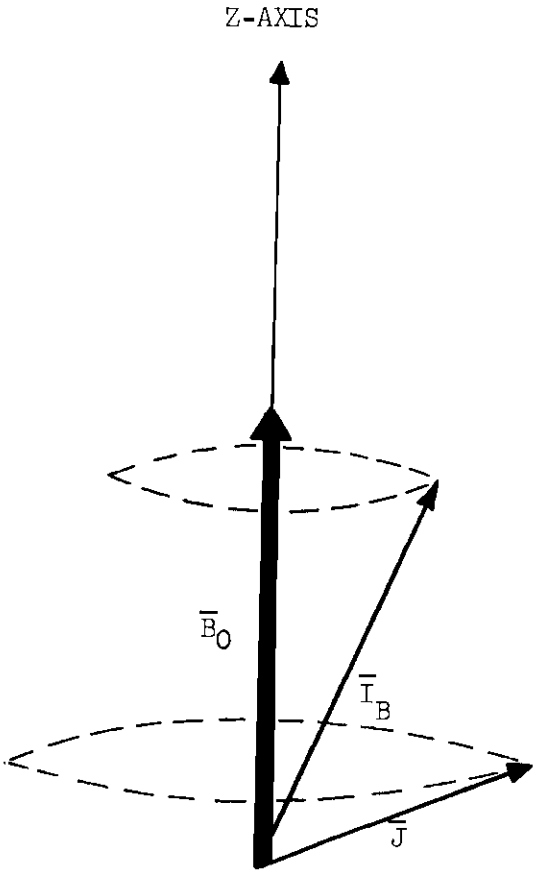

Figure 5. Decoupling of the Nuclear Angular Momentum. (Nuclear angular momentum $\bar{I}_B$ and the electron shell angular momentum $\bar{J}$ precess independently in the presence of a strong magnetic field.)

Static Electric Quadrupole Interaction

A homogeneous electric field exerts no torque on a nucleus since there are no nuclear electric dipole moments. It is possible for the quadrupole moment Q of a nucleus to interact with the existing electric field gradients. Such interaction between the nuclear electric quadrupole moment and the electric field gradient gives rise to precession of the angular momentum about the axis of the gradient field. The effects of such an interaction on the angular correlation process can be seen through the magnetic interaction analogy. Higher multipole effects can be neglected since they are much smaller than the quadrupole effect.

In this dissertation, the effects of the static magnetic fields on the directional correlations have been investigated. The static electric quadrupole interactions in liquid environments are believed to have negligible influence on the directional correlations as compared to the magnetic effects. In our decoupling experiments, the decaying nucleus was embedded in a liquid environment in order to reduce the influence of electric fields.

Purpose Of This Research

The purpose of this research was to search for the possible magnetic perturbation of gamma-gamma directional correlations in decays where the intermediate level has a half-life greater than about one nanosecond. This becomes especially important in the experimental determination of the ratio of reduced matrix elements, δ, for transitions of mixed multipolarity. Various nuclear models can predict these mixing parameters δ. In the absence of external perturbations

an accurate A_2 coefficient would yield a δ which should agree with the value that is predicted by a correct nuclear model.

Sb^{125} Problem

Low energy excited states of Te^{125} which result from the decay of Sb^{125} have been investigated by various authors. The pertinent portion of the decay scheme given by Stone et al. (14) and Inamura (15) is shown in Figure 6.

The lifetime of the 35.5 keV first excited state has been measured by Inamura to be 1.58 ± 0.15 nanoseconds. Marelius et al. (16) reported a value of 1.45 ± 0.03 nanoseconds. Electron conversion data obtained by Geiger et al. (17) and Mazets et al. (18) indicate little or no E2 admixture for the 35.5 keV transition to the ground state. These results have been confirmed by Salzberg (19) in directional correlation experiments.

There is still some disagreement on the value of the multipolarity of the 427 keV transition. Several values of this mixing parameter have been determined utilizing different experimental techniques. Stone et al. (14) performed nuclear orientation experiments and Wyly et al. (20) performed directional correlation experiments. The cause of discrepancy might be attributed to the possible attenuation of the directional correlation because of the 1.6 nanosecond lifetime of the 35.5 keV level. No previous experiments have been carried out with regard to investigating this possibility in this decay.

Sm^{153} Problem

Gamma rays in Eu^{153} following the decay of 47 hour Sm^{153} have been studied using various techniques including angular correlation experi-

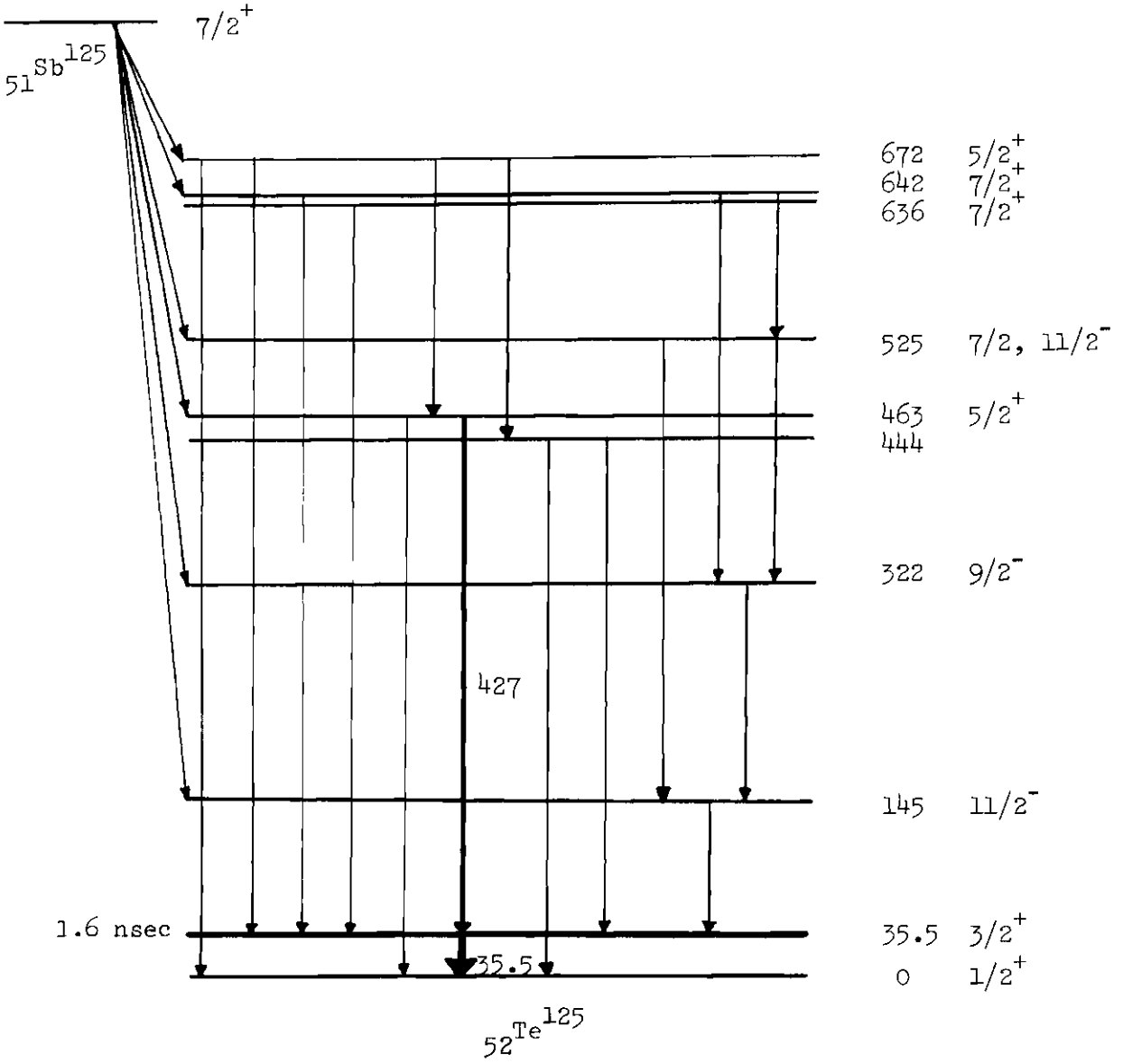

Figure 6. Pertinent Portion of the Decay Scheme of Sb^{125} Featuring the Low-lying Levels of Te^{125}

ments. Figure 7 shows the decay scheme of Eu^{153} as given by Ungrin and Johns (21). The half-life of the 103 keV level has been measured as 3.8 nanoseconds by Vergnes and Marty (22), by McGowan (23), and by Nainan (24). Beta-gamma and gamma-gamma coincidence experiments of Dubey et al. (25) were in agreement with the conclusion that 70 keV and 103 keV transitions may be of mixed type, namely M1 and E2. The conversion electron spectrum in Eu^{153} was studied by Graham et al. (26). From L-subshell ratios, they concluded that the 70 keV gamma ray was 98.2% M1 + 1.8% E2 and that the 103 keV gamma ray was 98.4% M1 + 1.6% E2. Sund and Wiedenbeck (27) in their directional correlation experiments give a value of $A_2 = 0.005 \pm 0.007$ for the 70-103 keV cascade. McGowan (28) also reports the radiation distribution to be isotropic within 3%. The possible attenuation of the 103 keV level has not been investigated prior to this work.

Ce^{143} Problem

The decay of 33.7 hour Ce^{143} to levels in Pr^{143} has been studied by a number of investigators (29, 30, 31) resulting in a fairly well established decay scheme (32) which is shown in Figure 8. The half-life of the 57 keV level has been measured to be 4.2 nanoseconds by Graham et al. (33). The atomic beam experiments of Budick et al. (31) established a spin of 7/2 for the ground state of Pr^{143}. Graham et al. (33) showed that the 57 keV transition was M1 + $\leq$ 0.3% E2 and that the 293 keV transition was (66 ± 16) % M1 + (34 ± 16) % E2 as a result of their measurements of the L-subshell internal conversion ratios. Gelletly et al. (34), on the basis of the same kind of measurements, reported a more accurate E2 admixture of (0.15 ± 0.03) % in the 57 keV

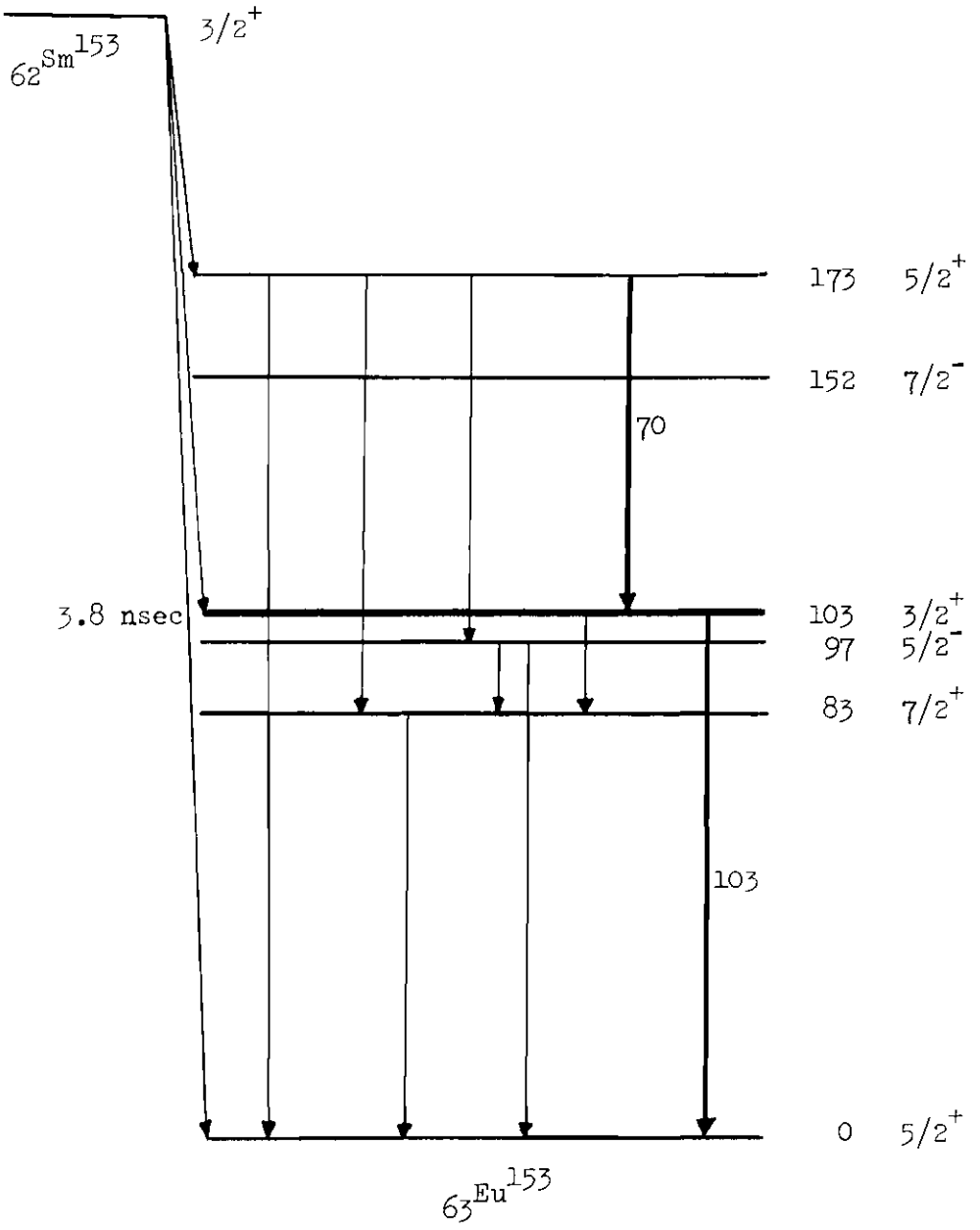

Figure 7. Pertinent Portion of the Decay Scheme of Sm^{153} Featuring the Low-lying Levels of Eu^{153}

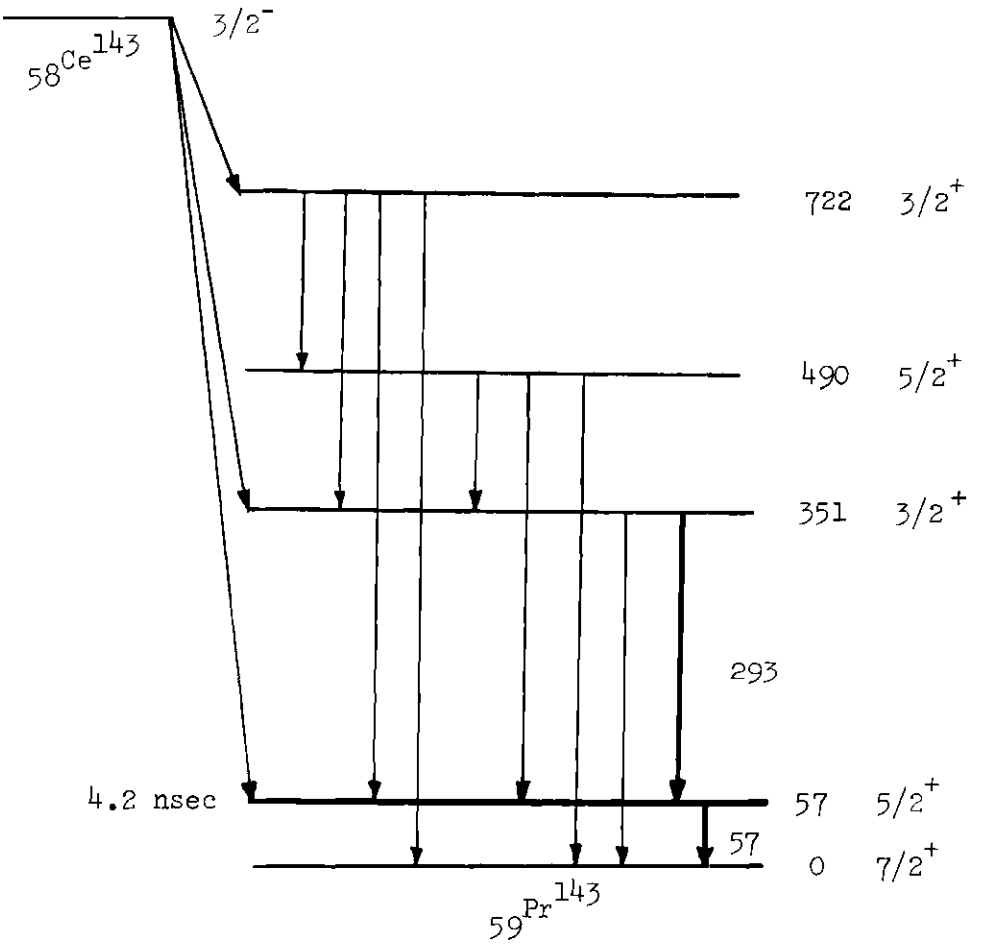

Figure 8. Principal Features of the Energy Level Scheme for Pr^{143}, Following Beta Decay of Ce^{143}

and (37 ± 4) % in the 293 keV transitions. This result for the 57 keV transition is in disagreement with the conclusions of Sunyar and Thieberger (35) and the discrepancy has been attributed by Gelletly et al. (34) to the possible attenuation of the 293-57 keV gamma-gamma directional correlation. Directional correlation experiments involving this cascade have been performed by various investigators. Simons et al. (36) report an A_2 coefficient of 0.106, Mancuso et al. (37) report A_2 = 0.123, Gopinathan (38) reports A_2 = 0.112, Bozek et al. (39) report A_2 = 0.132 and Levy (40) reports A_2 = 0.133. Gelletly et al. (34) reported that Sunyar and Thieberger's further studies on the time dependence of the 293-57 keV directional correlations have yielded an A_2 coefficient of 0.180 which was obtained by extrapolation of their results to zero time. Rotations of the 293-57 keV gamma-gamma integral directional correlation pattern have been measured by Sunyar and Thieberger (35) in a 7350 gauss field.

CHAPTER II

EXPERIMENTAL APPARATUS

The apparatus utilized in this dissertation consisted of an electromagnet, solid state and scintillation detectors, preamplifiers, amplifiers, single channel analyzers, fast-slow coincidence circuits and analog-to-digital converters (ADC) interfaced to a digital computer. The digital computer was also interfaced to a motorized turntable, clocks, various input and output devices and was programmed to collect data, to change the position of the movable solid-state detector, and to reduce the data after certain acceptability conditions had been fulfilled.

Gamma Detectors

Three solid state detectors and a scintillation counter were used in these experiments.

The first one was a coaxial 30 mm^2 X 3 mm lithium drifted silicon Si(Li) detector manufactured by Kevex Corporation. This detector showed an energy resolution of 390 eV FWHM (full width at half-maximum) at 6.4 keV and 790 eV at 122 keV. The detector had a 0.051 mm beryllium window in front and was attached to a 31 liter Dewar cryostat containing liquid nitrogen. The distance from the crystal to the outside window was 0.4 cm. The preamplifier was supplied by the manufacturer and was of the type 2000.

The second one was a five-sided coaxial, type LGC 3.5X lithium

drifted germanium, Ge(Li), detector manufactured by Nuclear Diodes, Inc. The 25.1 cm^3 crystal was of trapezoidal shape with an active front area of 905 mm^2. The entrance window was 0.5 mm thick aluminum and the n-region was 1.0 cm behind the entrance window. The energy resolution was 1.73 keV FWHM at 122 keV and 2.58 keV FWHM at 622 keV. The peak to Compton ratio for a Co^{60} source (maximum height of 1332 keV photopeak compared to maximum height of Compton edge) was 13 to 1.

The third detector was a 25.5 cm^3 Ge(Li) detector of coaxial type manufactured by the Ortec Corporation. This detector had an active front area of 892 mm^2 which was 0.5 cm behind the 0.5 mm thick aluminum window. The energy resolution was 2.1 keV FWHM at 1.33 MeV. The peak to Compton ratio for a Co^{60} source was 21 to 1.

The last detector that was used in these experiments was a scintillation counter consisting of a 3 X 3 inch Tl doped Sodium Iodide, NaI(Tl), crystal coupled to a RCA 8054 photomultiplier tube through a 10 cm long plastic light pipe. A combination of netic and conetic layers of magnetic shielding was wrapped around this detector to reduce magnetic effects on the electron trajectories in the photomultiplier tube.

All gamma detectors were shielded from various scattering effects by a layer of lead that was 0.5 cm thick.

Electronics

The electronics instrumentation used in these experiments was basically the same for the different isotopes that were being investigated. Details of the instrumentation are presented for each isotope.

Sb^{125} Experiment

A block diagram of the electronics involved in this experiment is shown in Figure 9. The output signal from the stationery NaI detector first passed through a series of preamplifiers and amplifiers. The main amplifiers provided bi-polar pulses for coincidence timing and energy analysis. The amplified pulses were split into two channels, one signal was sent into a single channel pulse height analyzer and the other into a fast coincidence circuit. Similarly, the output signals from the Si(Li) detector went through the same steps. The function of the fast coincidence circuit was to perform a time analysis on these signals. The leading edges of the incoming pulses were shaped into very narrow pulses and the resolution of the coincidence circuit was determined by the width of these pulses. When two such pulses from the two detectors overlapped, a signal generated by the fast coincidence circuit was sent to a slow coincidence circuit. The output of the NaI single channel analyzer, whose window was set to include only the 427 keV photopeak, was also sent to the slow coincidence circuit. The outputs of the slow coincidence circuit and the two single channel pulse height analyzers were fed into three scalers. The output signal from the Si(Li) amplifier went to the ADC which was gated by the signal from the slow coincidence circuit.

Analog-to-digital converters (ADC) of type NS-625 manufactured by Northern Scientific Corporation were used. The function of the ADC was to digitize the signal from the Si(Li) detector for processing by a digital computer. The data were then stored in the computer.

The fast coincidence resolving time was about 34 nanoseconds.

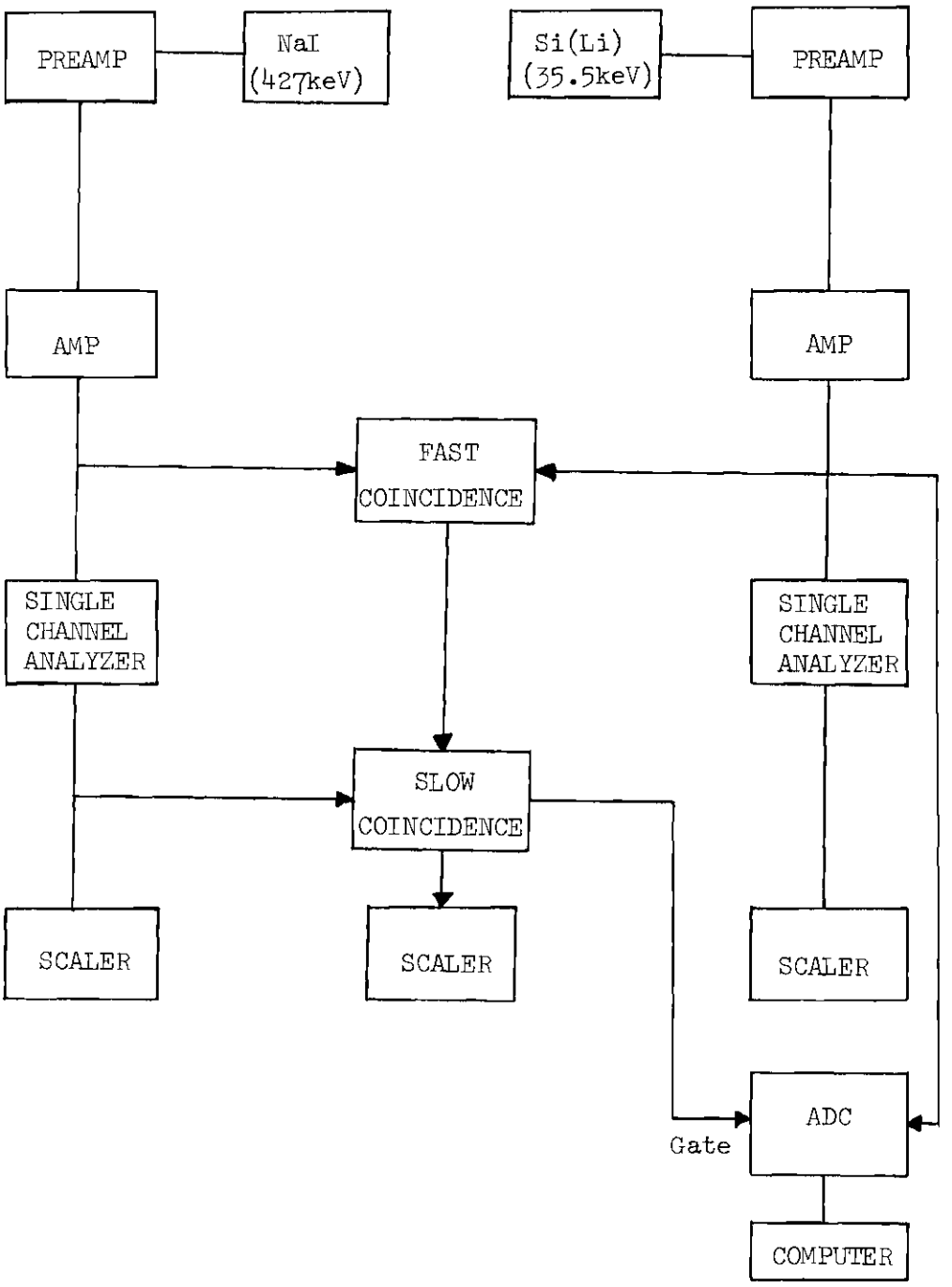

Figure 9. Block Diagram of the Electronics Involved in Sb^{125} Experiment

In order to measure the accidental coincidences, one input of the fast coincidence circuit was connected to a 500 nanosecond time delay switch. To verify that no reals were counted with the accidental coincidences, the following test was performed. The rate of accidental coincidences from a single source was compared to the rate from two different sources that were screened from one another. These rates were found to be the same.

Eu^{154} Experiment

The electronics diagram for this experiment is shown in Figure 10. A Ge(Li) detector (LGC 3.5X) was substituted for the movable Si(Li) detector. In this experiment slow coincidence requirements were placed on the output of both detectors. Only the photopeak due to the 1270 keV radiation was accepted but regions of the spectrum at higher and lower energies than the 123 keV photopeak were accepted. The resolving time of the fast coincidence circuit was 33 nanoseconds.

Sm^{153} Experiment

The electronics diagram for this experiment, Figure 11, shows that two Ge(Li) detectors were utilized. A slow coincidence requirement was imposed upon the output of the stationary LGC 3.5X detector. The corresponding single channel analyzer was set to accept the 70 keV photopeak. The resolving time of the fast coincidence circuit was 24 nanoseconds.

Ce^{143} Experiment

The electronics diagram in Figure 12 shows that a stationary NaI detector and a movable LGC 3.5X Ge(Li) detector were used in these experiments. A slow coincidence requirement was imposed upon the output

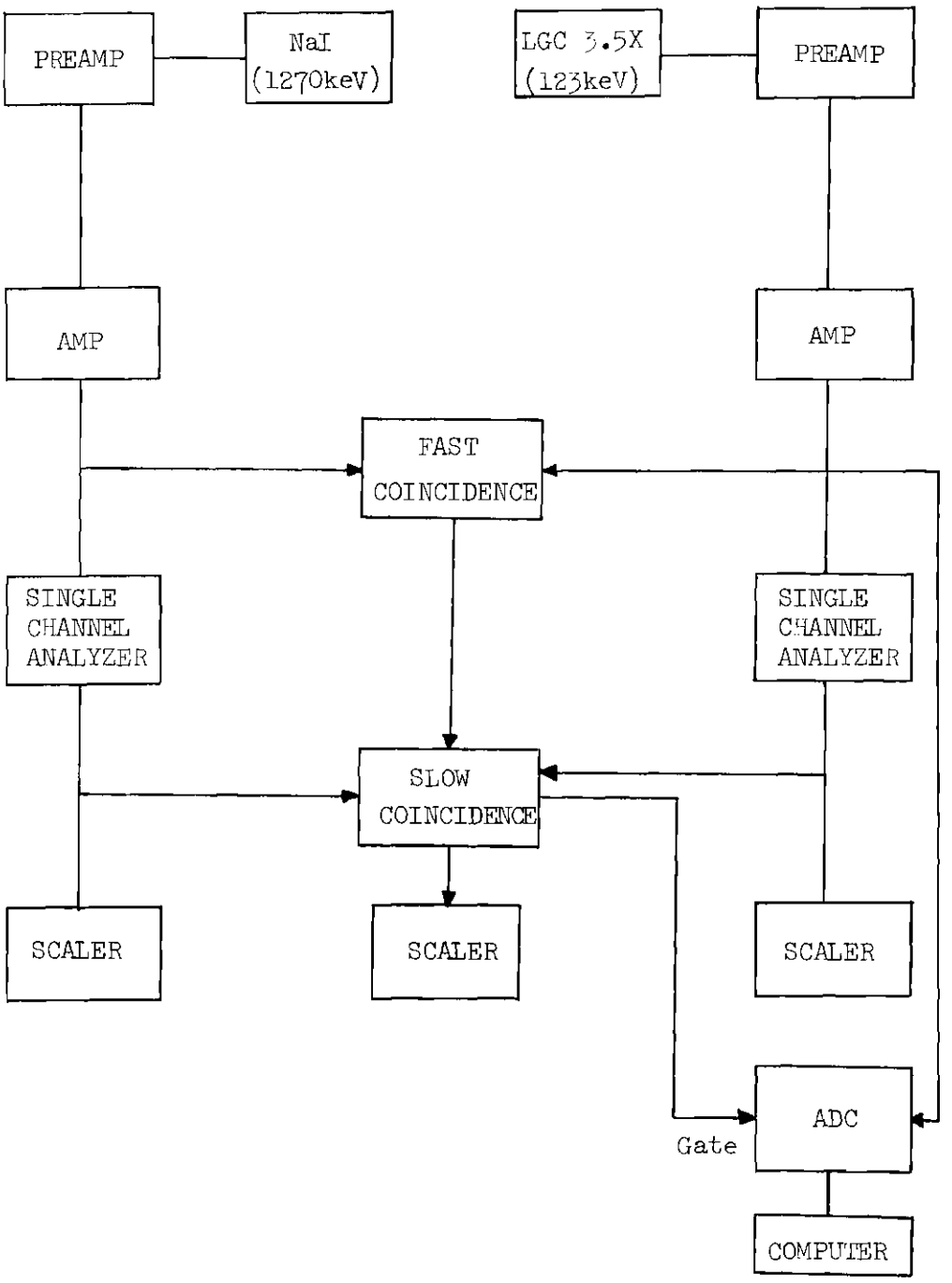

Figure 10. Block Diagram of the Electronics Involved in Eu^{154} Experiment

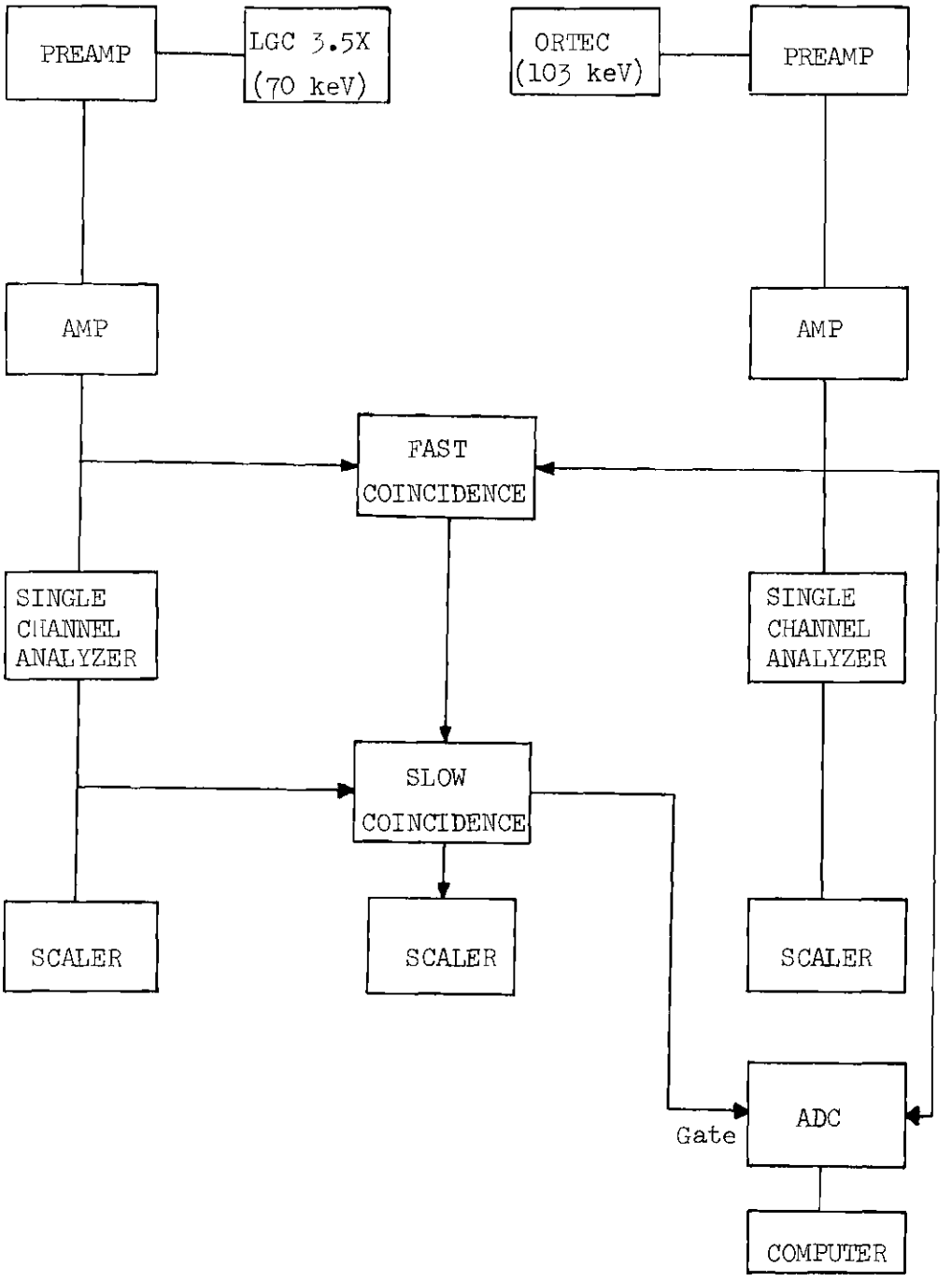

Figure 11. Block Diagram of the Electronics Involved in Sm^{153} Experiment

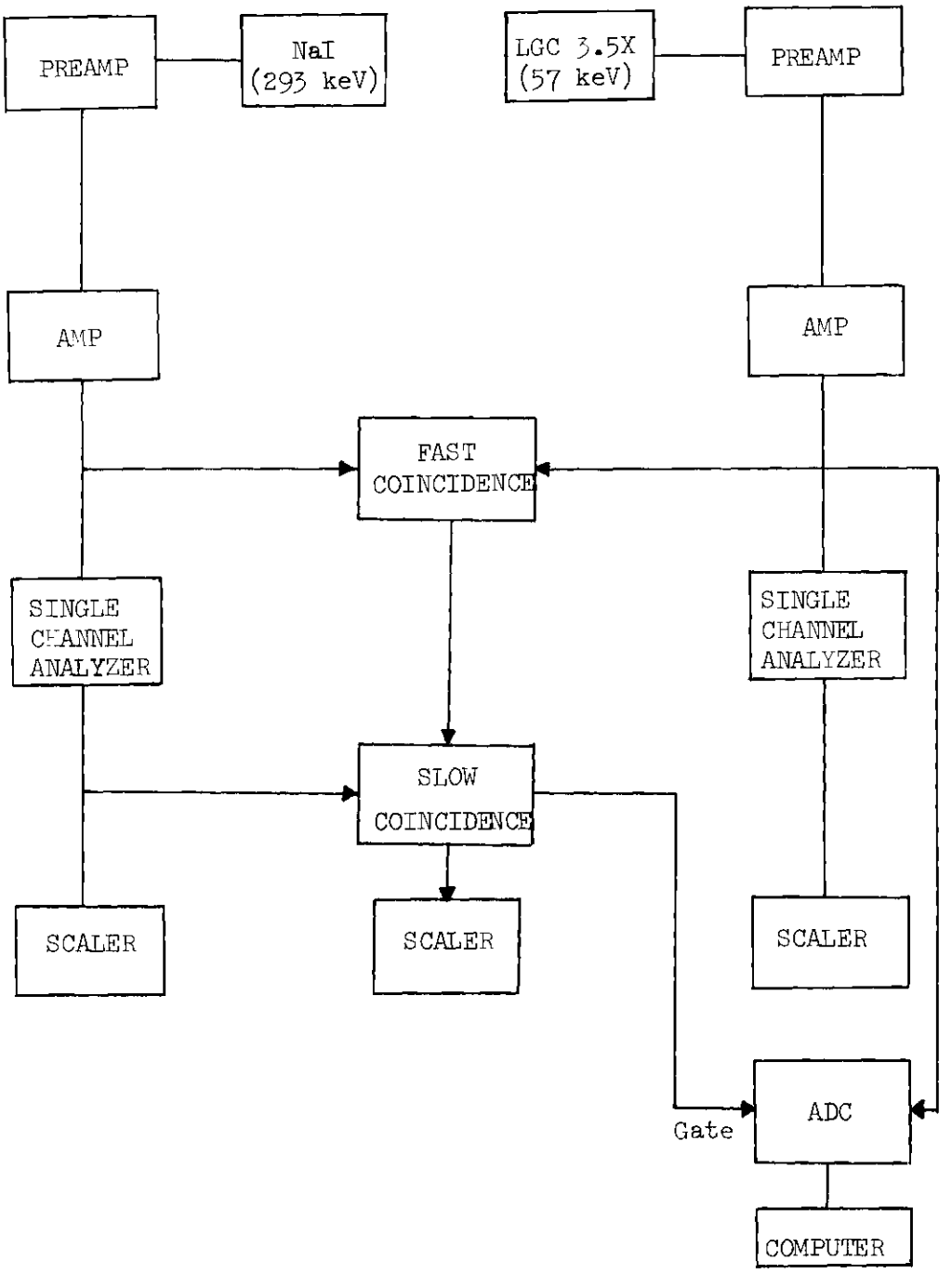

Figure 12. Block Diagram of the Electronics Involved in Ce^{143} Experiment

of the NaI detector and the corresponding single channel analyzer was set to include the region around the 293 keV photopeak. The fast coincidence resolving time was 25 nanoseconds.

Electromagnet

The electromagnet consisted of two hollow pole pieces, four coil forms and two end pieces. The magnetic path was of Armco ingot iron. The magnet was capable of producing fields up to 7800 gauss at 200 amperes. The electromagnet was cooled by circulating water through the winding which was copper tubing of nominal outside radius 1/8 inch. Shrinkable plastic tubing was used for insulation. There were four windings in parallel for water flow and in series electrically. A well regulated, water-cooled, three-phase power supply was used to energize the magnet.

Counting Geometry

In each one of these three experiments data were collected using a stationary detector and a movable detector. In our magnetic decoupling experiments data were collected with the movable detector set at 90°, 180°, and 270° with respect to the stationary detector, whereas in experiments performed without the magnet in place two additional positions, 135° and 225°, were included. In the Sb^{125}, Eu^{154} and Ce^{143} experiments the NaI detector was stationary whereas the Si(Li) or the Ge(Li) detector was movable. In the Sm^{153} experiment the LGC 3.5X Ge(Li) detector was stationary.

The movable detector was mounted on a turntable which was interfaced to the computer and a control program governed the rotation of the

turntable. Positioning of the movable detector was carried out utilizing phototransistors and small light bulbs mounted underneath the turntable. Whenever a light bulb was directly above a certain phototransistor, which corresponded to a selected angle code, an output signal was generated.

Computer And Data Collection Program

An on-line PDP-8 computer with 12,000 twelve-bit words of core storage made by Digital Equipment Corporation was used in this research to collect, sample and analyze data while the experiment was in progress. Additional memory capacity was provided by three random access magnetic disks with a capacity of 32,000 words each. Entering and storing information in core memory could be done either with the operator's console or a teletype unit. Other accessories included a display scope and high speed paper tape punch and reader.

The computer was operational on a foregound/background (41) basis which allowed one to use the computer while it was collecting data. Any program could be run simultaneously with the data collection. The foreground operation, which is also called the DATA program, was responsible for collecting, sampling and printing the data. This program was assigned 4000 words of core storage and 32,000 words of disk storage. The foreground operation required very little time from the processor since data from the ADC were stored in a "data break mode" which did not utilize the central processor. The DATA program assumed command of the computer for about 25 seconds out of 60 minutes of data collection time. The larger portion of this 25 second time interval was

taken up by the rotation of the table as the data processing time was very short. However, during this time interval, the background operation was completely halted. An essential feature of the system was a model KT-08 trap which trapped a number of instructions in the background mode so that such instructions would not interfere with the data collection program.

The computer program (42, 43, 44) may be divided into three parts. The first part dealt with the setting up of the experiment. The detectors could be turned on and off without permanently storing this information in the memory. Also, the spectrum observed could be displayed on an oscilloscope with the desired magnification. This part of the computer program was helpful in centering the source and making the necessary adjustments in the physical environment. The second part of the program was concerned with collecting, analyzing, storing and printing data. The program was capable of handling a maximum of six peaks. At the end of the first counting period an interrupt pulse from the clock suspended the counting momentarily and the collected data were stored as the reference data. Then the counter was rotated to a new position and the data collection resumed. At the end of the next time period another interrupt signal was given by the clock which initiated certain comparisons. The singles rates, coincidence rates, and locations of the peaks were compared with the reference data. The position of the counter was checked and if everything satisfied certain acceptability conditions, the data were accepted and data collection was resumed. Otherwise the data were rejected. In the event of data rejection, certain codes inserted in the program were usually helpful

in indicating the nature of the trouble. After each time period, the current data were averaged with accumulated data and stored in the disk memory. A log entry for each run was stored in the disk memory and was printed out at the end of each counting interval, if desired, to monitor the operation of all the equipment. The log entry included information such as the run number, angle code, data collection time, locations of peaks, and singles and coincidence rates (see Figure 13). Also at any time the desired coincidence spectrum, which is the coincidence rate divided by the singles rate in the movable counter at a given angle (which will be referred to as the normalized coincidence rate), could be printed out channel by channel over a range of about 64 channels.

The last part of the program was designed to make a least squares fit of Gaussian distributions plus linear background to the spectrum that was stored in the memory. This program could be carried out without interrupting the data collection program and it extracted the necessary data from the disk memory. This feature was very helpful since it allowed monitoring data collection and making comparisons between the data collected from one day to another while the experiment was still in progress. In using the fitting program (44), the coincidence spectrum was displayed on the scope giving the choice of deciding how many parameters to use in order to make the best possible fit. The first cycle of the program plotted the parameterized curve as well as the data points for the visual comparison, computed the deviation, and waited for the instruction to start the least squares fit program. In the event that the initial parameters were not suitable, another set of parameters could be typed in and a new deviation calculated until the

```
RF 0200 +0.2230666E+01 0200 +0.2526666E+01
  0273 0010 0400 +0.1987722E-01 0000 0034


0001 0004 + 3000
  0275 0000 0210


0002 0006 + 3000 +1.006 + .990 + .891 + .000
  0274 0000


0003 0004 + 3000 + .970 + .973 +1.030 + .000
  0274 0000


0004 0002 + 3000 + .960 + .961 + .948 + .000
  0274 0000


0005 0004 + 3000 + .947 + .949 +1.102 + .000
  0274 0000


0006 0006 + 3000 + .945 + .942 +1.011 + .000
  0274 0000


0007 0004 + 3000 + .913 + .925 +1.110 + .000
  0274 0000


0010 0002 + 3000 + .906 + .915 + .925 + .000
  0274 0000


0011 0004 + 3000 + .896 + .904 + .877 + .000
  0274 0000
```

Figure 13. Typical Log-Entry Printout

experimenter was satisfied. Then the least squares program would be started. At the end of each cycle the deviation was printed out and the two curves were displayed on the scope. Further details of the fitting program are discussed in Appendix B.

CHAPTER III

INVESTIGATION OF POSSIBLE PERTURBATIONS

Preliminary investigations were directed towards checking the experimental apparatus. The experiment of Stiening and Deutsch (9) on the decoupling effects of a longitudinal magnetic field on the 1270-123 keV directional correlation in the decay of Eu^{154} was repeated. After observing the decoupling effect of an external magnetic field in Eu^{154}, similar experiments were carried out with Sb^{125}, Sm^{153} and Ce^{143}. Results of these experiments will be presented in this chapter in four sections.

Eu^{154} Experiment

The 16 year Eu^{154} was prepared by the Oak Ridge National Laboratory in the form of $EuCl_3$ in HCl solution. The production method was the capture of low energy neutrons by an Eu^{153} target. The Eu^{154} isotope was deposited in a cylindrical plexiglass container in liquid form. This container had a 5 mm inside diameter, a 5.5 mm outside diameter and was 25.0 mm long. The sample was then suspended between the poles of the electromagnet with the cylindrical axis perpendicular to the plane of the turntable. The column of liquid inside the tube was about 1 mm high. The main features of the level scheme of Gd^{154}, following the decay of Eu^{154}, are shown in Figure 14.

The 1270-123 keV cascade was investigated using the stationary 3 X 3 inch NaI detector and the movable LGC 3.5X Ge(Li) detector. These

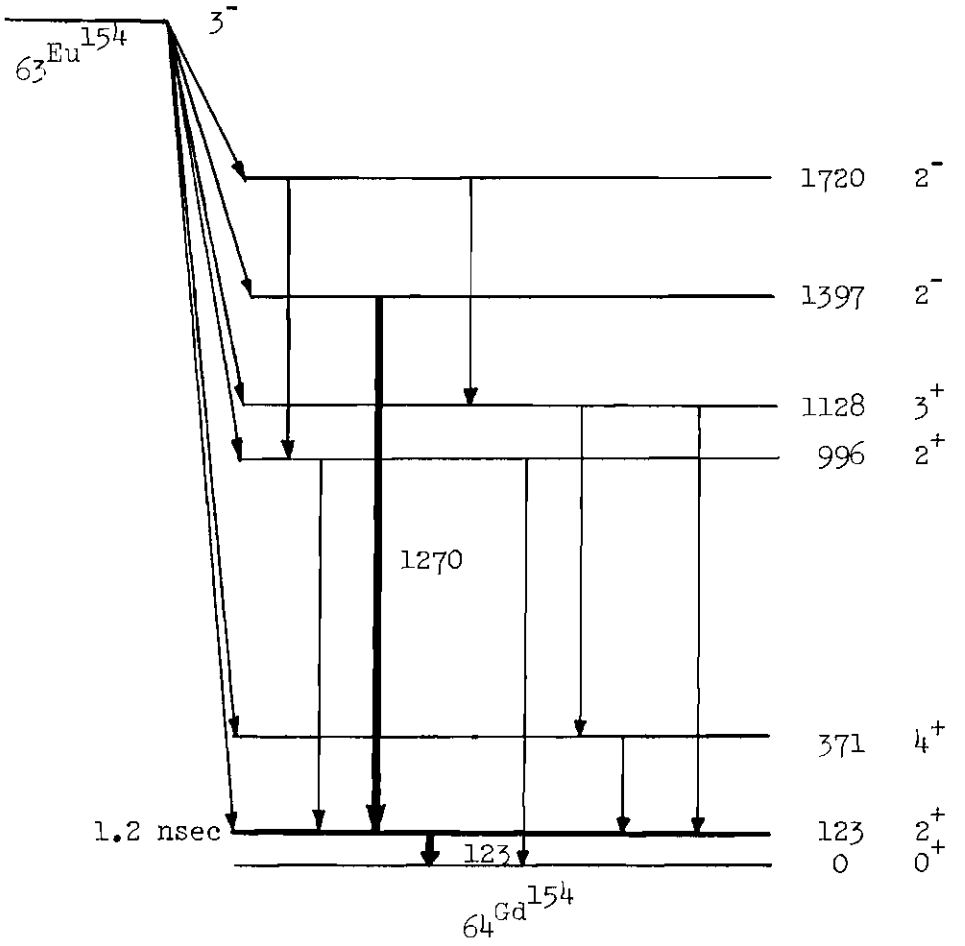

Figure 14. Principal Features of the Energy Level Scheme for Gd^{154}, Following the Beta Decay of Eu^{154}

detectors were 10 cm and 6 cm away from the source, respectively. The source was centered until the singles rates in the Ge(Li) detector differed at most by 1% at the 90°, 180° and 270° positions. The single channel pulse height analyzer window in the NaI detector channel was set to include the 1270 keV gamma peak. The Ge(Li) output to the ADC was gated by the slow coincidence output. The electronics diagram is given in Figure 10.

The pertinent portion of the coincidence spectrum of the 123 keV gamma ray which was observed in the Ge(Li) detector at the 180° position is given in Figure 15. This spectrum showed a higher background compared with the 90° and 270° positions. The occurence of cross-talk between the detectors was considered possible in addition to the scattering of the gamma rays as they pass through the conical aperture in the pole piece of the electromagnet. Heavy lead shielding was wrapped around the detectors and lead apertures of 4 cm diameter were placed in front of them. It was observed that this asymmetry in the background was reduced as the thickness of the lead aperture was increased. Apertures that were 8 mm thick were finally used in front of the detectors.

The strong magnetic fields utilized in this experiment produced shifts in the amplitude of the 1270 keV gamma peaks in the NaI detector. This effect was minimized by two methods. First, a plexiglass light pipe of length 10 cm was inserted between the NaI crystal and the photomultiplier tube so that the latter would be further away from the magnetic fields. Then a combination of conetic and netic shielding was used to further reduce such shifts. Finally, the energy selector dial on the output of the NaI detector was adjusted at each field strength

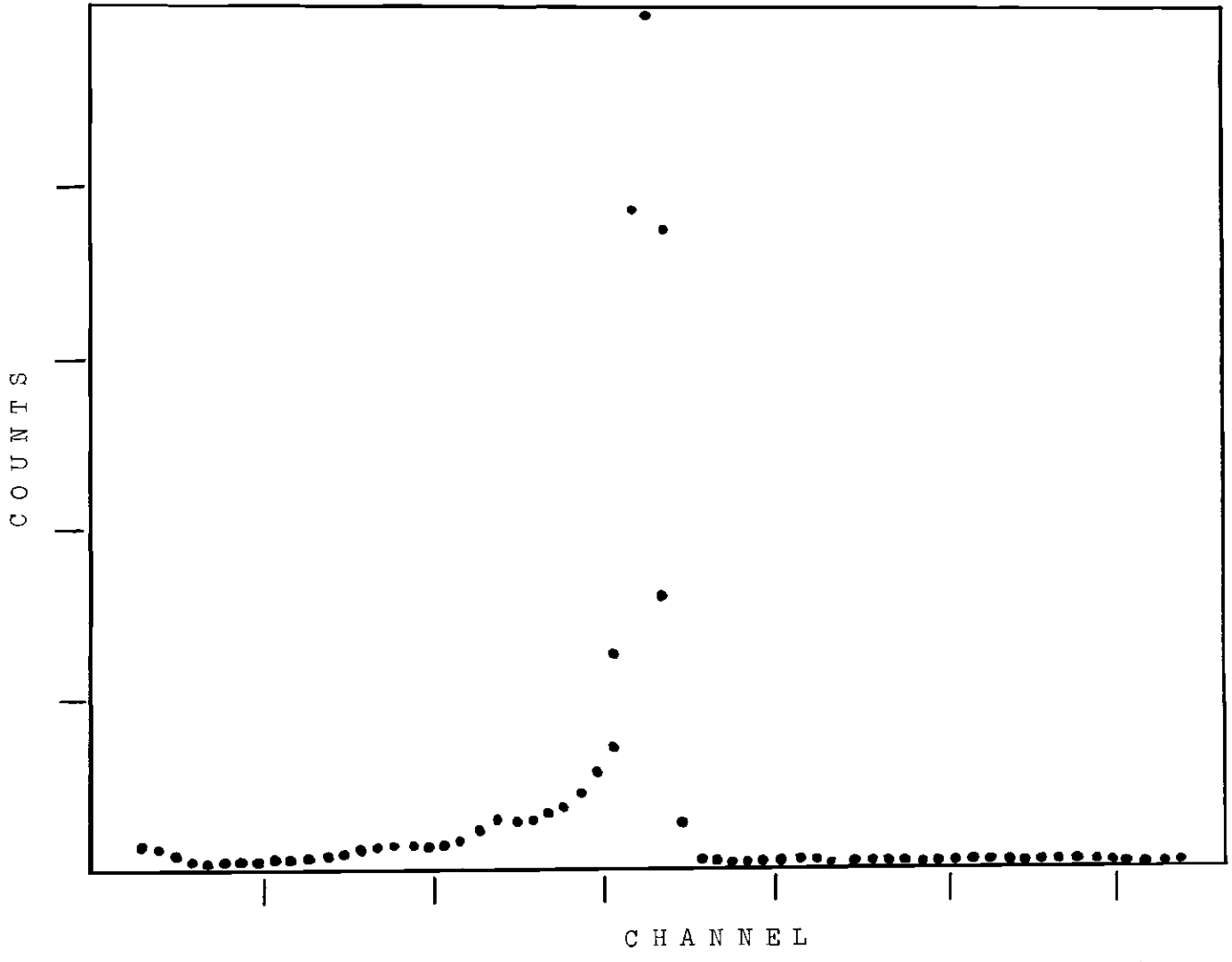

Figure 15. Pertinent Portion of the 1270-123 keV Coincidence Spectrum in Eu^{154} at 180° Position

in order to compensate for the residual effect.

Accidental coincidences were measured by the introduction of a 0.5 microsecond delay in the Ge(Li) channel.

The data of this experiment were analyzed using the FIT0 and FIT1 programs which essentially calculated the area under the coincidence peak by applying a least squares fit of a Gaussian distribution plus linear background. The coincidence rates for each angle at different magnetic field strengths, namely 60, 500 and 6000 gauss, were calculated.

These results are summarized in Table 1. The second order directional correlation coefficient, A_2 corrected for detector geometry by the factor 0.901, is also shown. A definite magnetic decoupling effect was observed as the magnetic field strength was increased to 6000 gauss.

Sb^{125} Experiment

After observing the effect of the decoupling magnetic field in Eu^{154}, the 427-35.5 keV cascade in Sb^{125} (see Figure 6) was investigated utilizing a generally similar experimental set up.

The 2.7 year Sb^{125} source was prepared by the Oak Ridge National Laboratory. Ten-day Sn^{125} was produced by neutron capture in Sn^{124}. Sn^{124} decays into Sb^{125} through beta emission. This isotope, which was 99% pure in the form of $SbCl_3$ and SbOCl in HCl solution, was contained in a cylindrical plexiglass source holder which had an inside diameter of 5 mm, outside diameter of 5.5 mm and length of 2.5 cm. The stationary NaI and the movable Si(Li) detectors were 9.5 cm and 5.5 cm from the source center, respectively.

The single channel pulse height analyzer window in the NaI channel

Table 1. Summary of Decoupling Experiments Involving 1270-123 keV Cascade in Eu^{154}. (Total number of observed coincidences and the coincidence counting rates are given at each angle. The asymmetry column gives the ratio of the coincidence rate at 90° to that of 270°. F_{180} is the ratio of the true coincidences at 180° to the average of true coincidences at 90° and 270° (see Equation B.2).)

FIELD IN GAUSS	90°		180°		270°		ACCIDENTALS		ASYMMETRY	RATIO OF REALS TO ACCIDENTALS	F_{180}	A_2 (CORRECTED)
	COUNTS	RATE	COUNTS	RATE	COUNTS	RATE	COUNTS	RATE				
60	10,324	4232	25,873	5387	9,836	4098			1.03	15	1.32	0.21
500	7,732	4282	20,734	5495	7,301	4056			1.06	16	1.34	0.23
6000	9,875	4702	25,492	6070	9,295	4426	1,774	332	1.06	17	1.36	0.24±0.02

was set to include the 427 keV gamma peak. The coincidence spectrum of the 35.5 keV gamma ray and the 27 keV Te X-rays with the 427 keV gamma peak was observed. The output of the Si(Li) amplifier was fed into the ADC which was gated by the output of the slow coincidence circuit (see Figure 9). The pertinent portion of this coincidence spectrum is shown in Figure 16, which was obtained at the 180° position. This coincidence spectrum showed a higher background at the 180° position as compared with the 90° and 270° positions. Cross-talk between the detectors as well as other scattering effects were again considered in this experiment. Lead shielding was wrapped around the detectors and lead apertures were placed in front of them in order to reduce these effects.

Although our objective was to investigate the perturbation of the 427-35.5 keV cascade by an external static magnetic field, a simultaneous measurement of the directional correlation of the 427 keV gamma rays in coincidence with 27 keV Te X-rays was made. The latter cascade was expected to give isotropic results. Since the statistical precision in this case was much better than for the 427-35.5 keV directional correlation, the X-ray experiment was a good indicator of experimental difficulties that might have occurred.

With a magnetic field of 0.4 gauss, the directional correlation experiment was run until about 13,500 counts were collected under the 427-35.5 keV coincidence peak at the 180° position. The X-rays were found to be isotropic. Then a magnetic field of 6000 gauss was applied. This field produced a slight shift in the amplitude of the 427 keV pulses in the NaI detector. However, similar to the Eu^{154} experiment, this effect was compensated for by adjusting the energy selector dial in the

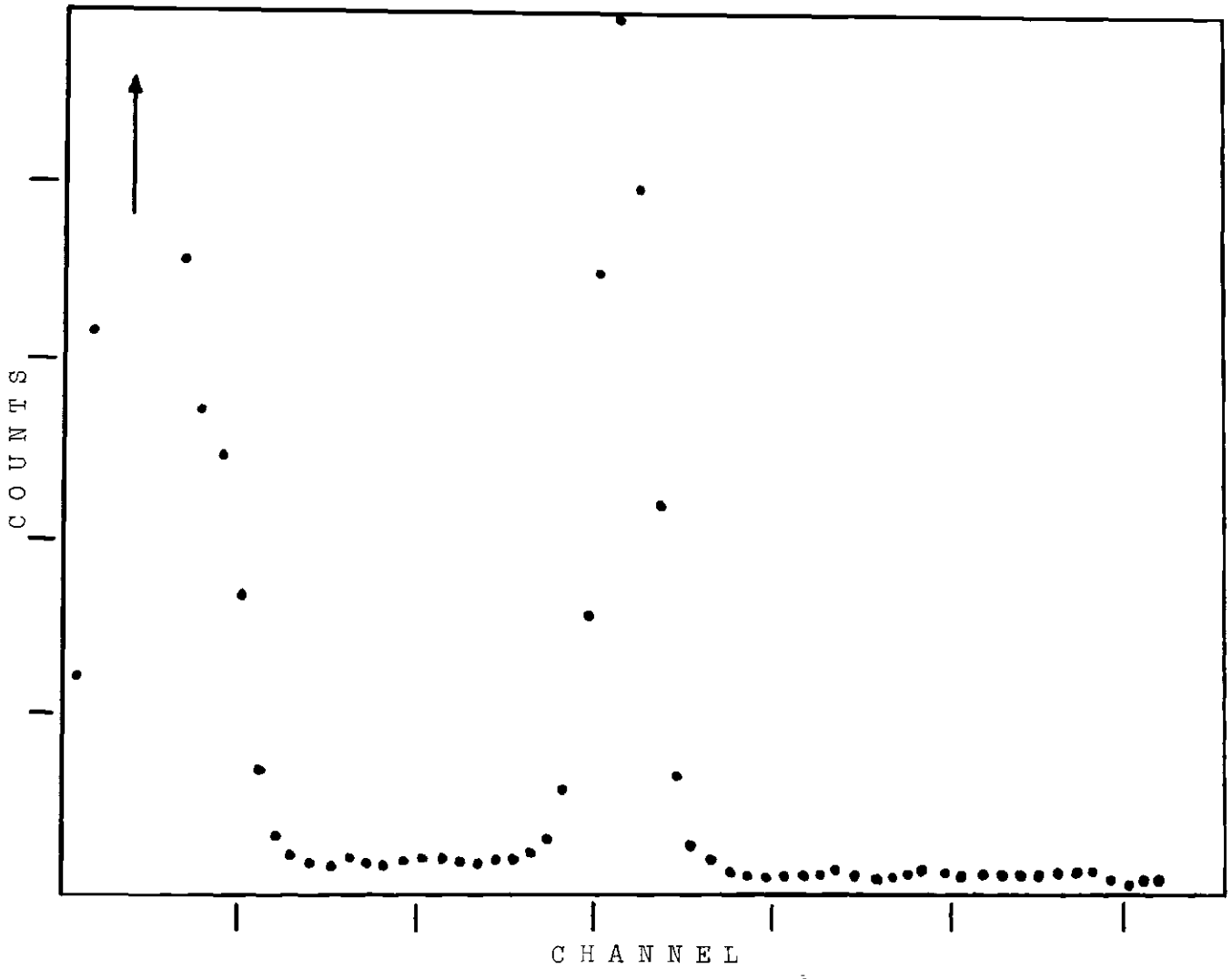

Figure 16. 427-35.5 keV Coincidence Spectrum in Sb^{125} as Observed at the 180° Position

NaI channel. Data were again accumulated and the X-rays found to be isotropic under the influence of the magnetic field.

Accidental coincidences were measured by insertion of a 0.5 microsecond delay in one channel. The accidental rates were determined with the field turned on and off. No difference was seen within the experimental error.

The results, which are summarized in Table 2, indicate that the A_2 value obtained for the two cases of a vanishing field and a 6000 gauss field are the same within the experimental error. No decoupling effect has been observed. The A_2 coefficient, corrected by a geometrical factor of 0.929, was found to be 0.19 ± 0.04.

Sm^{153} Experiment

The 47 hour Sm^{153} source was prepared at the Georgia Tech Nuclear Reactor in the form $SmCl_3$ in HCl solution. Sm^{152}, which was obtained from the Oak Ridge National Laboratory, was irradiated by thermal neutrons for about 1 to 2 minutes. The Sm^{153} source was sealed inside a cylindrical plexiglass container that was 2.5 cm long with inside and outside diameters of 5 mm and 5.5 mm, respectively.

The 70-103 keV cascade (Figure 7) was investigated in two sets of experiments. First, as in the Eu^{154} and Sb^{125} experiments, the source was placed between the poles of the electromagnet and decoupling experiments were performed. Two Ge(Li) detectors were used and the movable Ortec Ge(Li) detector was set to include the gamma spectrum near the 103 keV photopeak. A slow coincidence requirement was imposed upon the output of the LGC 3.5X Ge(Li) detector and the corresponding single

Table 2. Summary of Decoupling Experiments Involving the 427-35.5 keV Cascade in Sb^{125}

FIELD IN GAUSS	90°		180°		270°		ACCIDENTALS		ASYMMETRY	RATIO OF REALS TO ACCIDENTALS	F_{180}	A_2 (CORRECTED)
	COUNTS	RATE	COUNTS	RATE	COUNTS	RATE	COUNTS	RATE				
0.4	5,240	1248	13,455	1495	5,337	1244			1.00	2.7	1.30	0.19
6000	5,528	1228	13,134	1480	5,642	1254	2,533	402	0.98	2.7	1.29	0.19±0.04

channel analyzer was set to accept the 70 keV peak. These detectors were 6.0 cm and 7.0 cm away from the source, respectively.

With the exception of the utilization of two Ge(Li) detectors, the electronics were the same as in the Sb^{125} experiment (see Figure 11). The Ortec detector was found to be extremely sensitive to 5000 gauss fields at the source and it would not perform when placed at a distance of 5.5 cm from the source. Extra layers of conetic and netic magnetic shielding were wrapped around this detector so that no variation in the singles rate was observed with magnetic field. Lead shielding was again wrapped around both counters in order to minimize scattering effects.

Preliminary experiments were performed at different times after the sample had been irradiated by slow neutrons. A very prominent background hump was observed consistently, with or without a 6000 gauss field, in the data that were collected starting 1 hour after irradiation. Other experiments that were started between 48 and 72 hours following irradiation gave consistent results and the background hump decreased. A comparison of coincidence spectra for two experiments which were started 1 and 72 hours after irradiation, respectively, can be seen in Figure 17.

When a least squares fit, using two Gaussians and a linear background, was made to the data points collected in the experiment which started 1 hour after neutron irradiation, the areas under the two Gaussian peaks were found to be about the same. However, a similar fit made to the data points of an experiment which started 72 hours after irradiation gave a ratio of 1:3. After 100 hours the sample became too

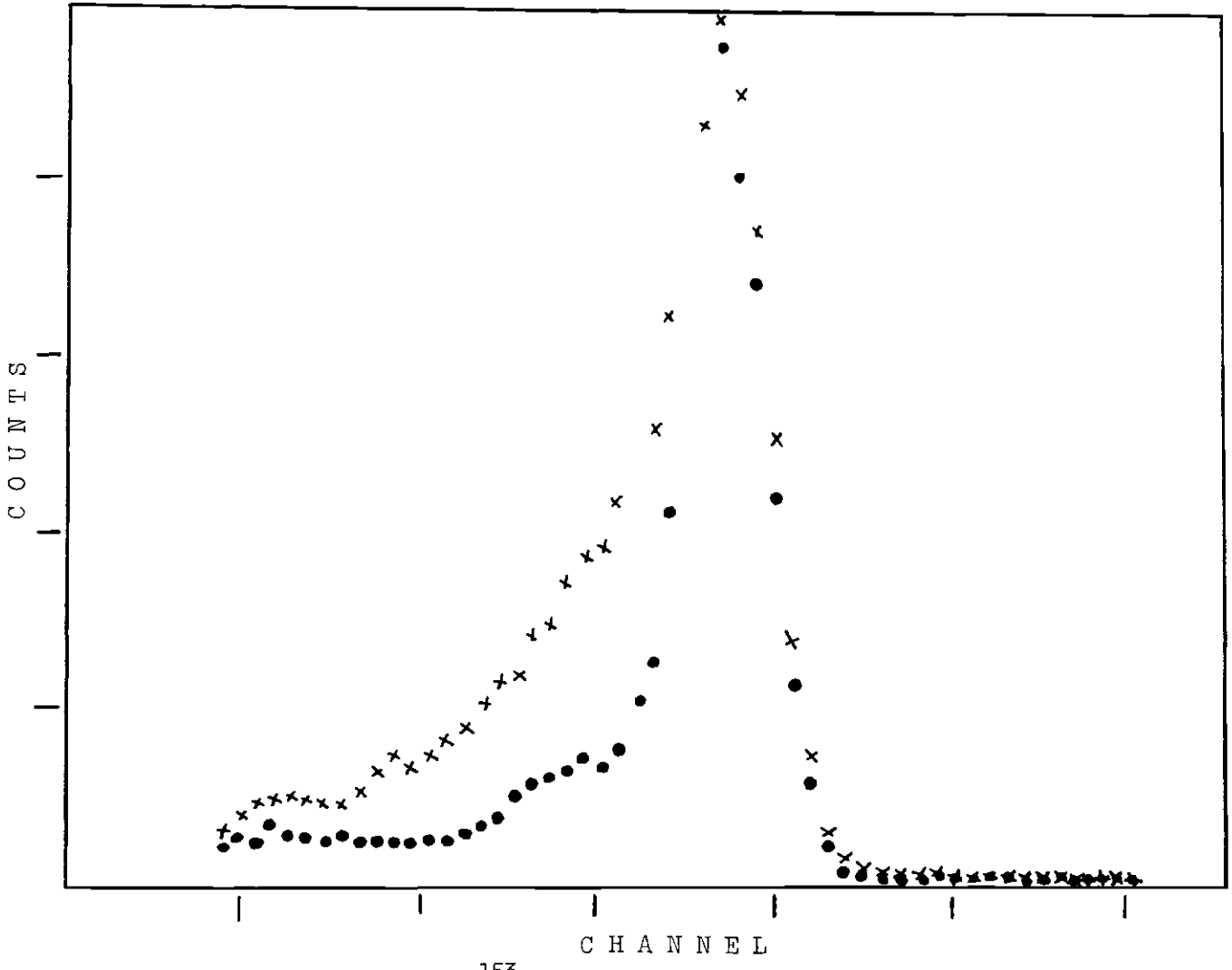

Figure 17. Coincidence Spectra for Sm^{153} at 180° Position. (Dots refer to data points collected 72 hours after irradiation and crosses to data points collected 1 hour after irradiation.)

weak for data collection.

Based on these preliminary results, it was deemed that a suitable time to start collection of data would be about 48 hours after irradiation. After such time the hump in the background (which is presumably due to some impurity decaying faster than Sm^{153}) would be minimized and could be subtracted reliably from the main peak to give the true coincidences.

The accidental coincidences played an especially important role in this experiment. After taking a complete cycle of real coincidence counts, twice at 180°, once at 90° and once at 270°, a complete cycle of accidental counts was taken. Then, another cycle of real coincidences was taken. Finally, another complete cycle of accidental counts was taken and these were averaged with the previous accidentals.

The results of the decoupling experiments are summarized in Table 3 and no effect of the magnetic field is noted. The correlation is found to be isotropic within the experimental error. The geometrical correction factor is 0.932.

In order to further verify that the directional correlation was nearly isotropic, a second set of experiments was conducted. The electromagnet was removed and the necessary changes in the environment were made to collect data. Removal of the magnet allowed one to collect data at two more positions, 135° and 225°. Three experiments were carried out. The first one started 47 hours after neutron bombardment. The second and the third experiments were performed on a new source and were started about 47 and 70 hours after irradiation, respectively. The average results of the three experiments are summarized in Table 3.

Table 3. Results of Sm^{153} Experiments Involving the 70-103 keV Cascade

FIELD IN GAUSS DECOUPLING EXPERIMENTS	90°		180°		270°		ACCIDENTALS		ASYMMETRY	RATIO OF REALS TO ACCIDENTALS	F_{180}	A_2 (CORRECTED)
	COUNTS	RATE	COUNTS	RATE	COUNTS	RATE	COUNTS	RATE				
0	9,236	2583	17,838	2573	9,876	2551	4,612	730	1.01	2.5	1.00	0.00
6000	8,511	5348	18,539	5483	10,827	5413	2,609	1631	0.99	2.4	1.03	$0.02^{+}_{-}0.03$

EXPERIMENTS WITH NO MAGNET	(90°+270°)/2		180°		(135°+225°)/2		ACCIDENTALS		RATIO OF REALS TO ACCIDENTALS	F_{135}	F_{180}	A_2 (CORRECTED)	A_4 (CORRECTED)
	COUNTS	RATE	COUNTS	RATE	COUNTS	RATE	COUNTS	RATE					
	10,621	1063	18,604	1034	11,727	1072	7,584	473	1.2	1.02	0.95	$^{+}_{-}0.02$ $^{+}_{-}0.04$	$^{+}_{-}0.06$ $^{+}_{-}0.06$

The results are again consistent with an isotropic correlation. The geometrical correction factors are 0.932 for A_2 and 0.719 for A_4.

Ce^{143} Experiment

Samples of 33 hour Ce^{143} were prepared by irradiating approximately 1 mg of Ce_2O_3 at a thermal neutron flux of 10^{13} cm^{-2} - sec^{-1} for 4 to 12 hours at the Georgia Tech Nuclear Reactor. Ce^{143} was dissolved in concentrated sulphuric acid and then sealed inside a plexiglass container in solution form.

Experiments were performed both with and without the magnet in place in order to investigate the 293-57 keV cascade (Figure 8). The same detectors were used in both types of experiments. The 3 X 3 inch NaI detector was stationary and the LGC 3.5X Ge(Li) detector was movable. As shown in Figure 12, a slow coincidence requirement was imposed upon the output of the NaI detector and the corresponding single channel analyzer was set to include the region around the 293 keV photopeak.

In our preliminary experiments, heavy lead and magnetic shieldings were wrapped around the counters. After several experiments were performed the results indicated that the lead shielding did not serve to minimize the scattering effects. In fact, it sometimes enhanced the background at the 180° position when the source activity was high. For this reason, the lead shielding around the counters was removed.

Directional correlation experiments with no magnet in place started as soon as the source became available after 4 hours of neutron bombardment. Data were collected for a span of 24 hours at 90°, 135°, 180°, 225° and 270° positions. The counting time was 500 seconds at

each position. As in the Sm^{153} experiments, the accidental coincidences played an important role and were recorded at the beginning, at the mid-point and at the end of each experiment. Approximately 10,000 coincidences were recorded at the 180° position and a least squares fit of a Gaussian distribution plus a linear background was made to the data points. The directional correlation coefficients were found to be $A_2 = 0.12 \pm 0.03$ and $A_4 = -0.09 \pm 0.12$. The geometrical correction factors are 0.718 for A_2 and 0.311 for A_4.

Magnetic decoupling experiments were performed utilizing magnetic field strengths of 0, 3000, 5000, 6200 and 7800 gauss. The pole pieces of the electromagnet were slightly modified which enabled us to obtain stronger fields. In some experiments the source was irradiated for 4 hours and in others for 12 hours, the latter giving us more time for an experiment. The results, after the removal of lead shielding, proved to be independent of the source activity. Data were collected at 90°, 180° and 270° positions with counting time being either 500 or 1000 seconds at each position. Depending on the activity, the experiments lasted between 5 and 20 hours. A coincidence spectrum as recorded by the Ge(Li) detector in the vicinity of the 57 keV gamma peak at the 180° position is given in Figure 18. Computation of the A_2 coefficients for different field strengths resulted in the appearance of a definite decoupling effect. Our results averaged over the number of experiments at a given field value are given in Table 4. The geometrical correction factor is 0.850. The unperturbed A_2 was inferred to be 0.18 ± 0.02. The low accidental rate in the last experiment was due to the fact that data were taken with a weak source.

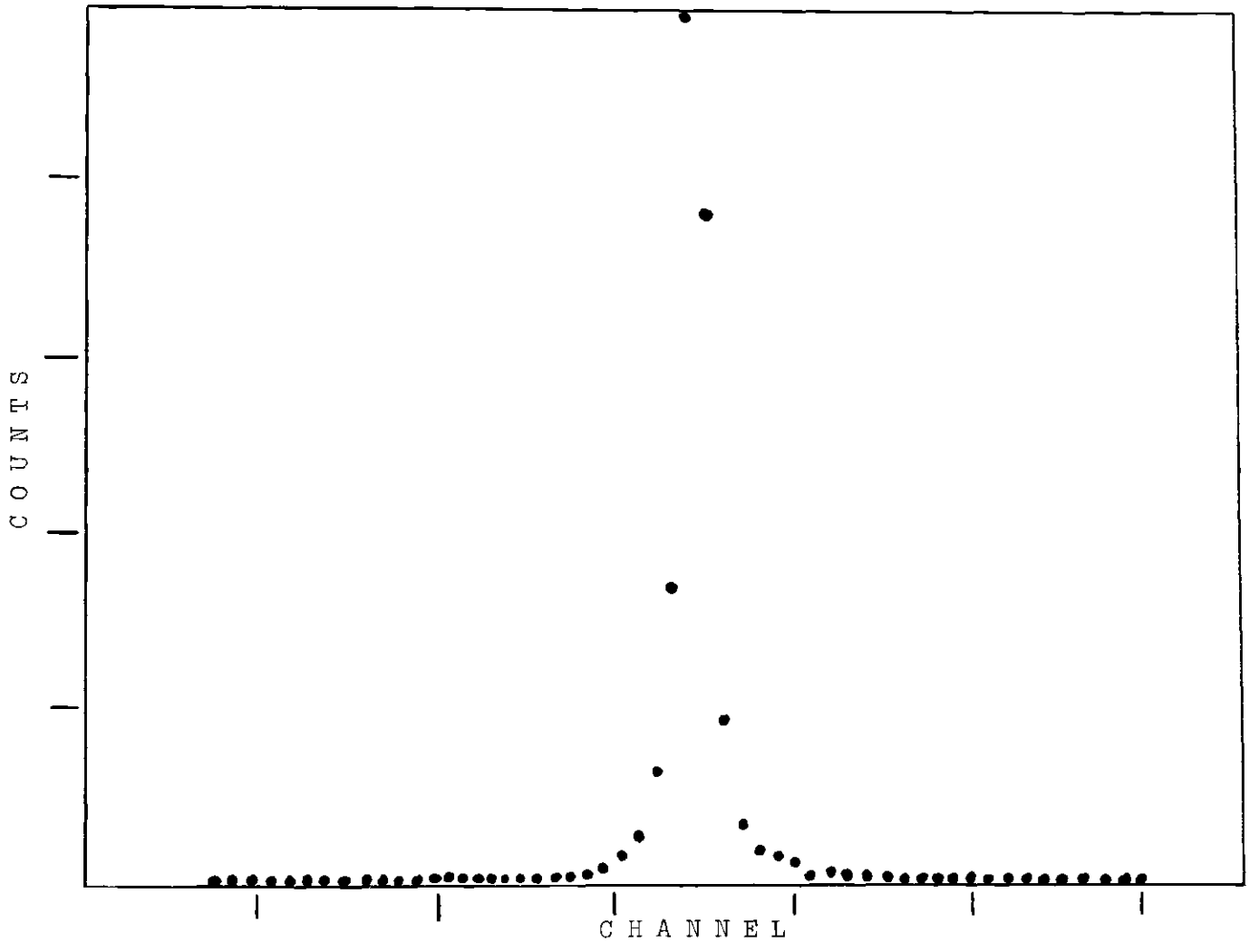

Figure 18. 293-57 keV Coincidence Spectrum in Ce^{143} at 180° Position with B = 0 Gauss

Table 4. Results of the Ce^{143} Experiments Involving the 293-57 keV Cascade

FIELD IN GAUSS	90°		180°		270°		ACCIDENTALS		ASYMMETRY	RATIO OF REALS TO ACCIDENTALS	F_{180}	A_2 (CORRECTED)
	COUNTS	RATE	COUNTS	RATE	COUNTS	RATE	COUNTS	RATE				
0	8,176	1487	18,840	1639	7,794	1417	1,710	171	1.05	9	1.15	0.11
3000	3,740	534	9.170	611	3,662	523	490	25	1.02	23	1.16	0.12
5000	7,117	1423	18,689	1700	7,964	1445	1,000	195	0.99	8	1.22	0.16
6200	7,207	1802	15,116	2159	6,290	1797	517	259	1.00	7	1.23	0.17
7800	4,961	413	11,632	509	5,116	409	267	9	1.01	56	1.24	0.18 ± 0.02

CHAPTER IV

INTERPRETATION OF RESULTS AND CONCLUSIONS

The purpose of these experiments has been to investigate the possible attenuation of the directional correlation coefficients due to static magnetic fields. Our efforts have been directed towards removing the attenuations in these coefficients.

The relatively high susceptibility of rare earth elements, with relaxation times of the order of 10^{-12} second, suggests that the gamma-gamma directional correlations may be magnetically attenuated in a liquid source. Günther and Lindgren (45) have derived a general formula for the increase of the effective magnetic field at the nucleus over the external field in a paramagnetic material which involves the "paramagnetic correction factor," β, where $\beta = 1+X$ and X is the magnetic susceptibility for the rare earth elements at the appropriate temperature. The factors for the rare earth ions of interest to the present work are listed in Table 5.

Eu^{154} Experiments

Our magnetic decoupling experiments involving the 1270-123 keV cascade were directed towards checking the experimental apparatus and comparing results with those of Stiening and Deutsch (9). We found (see Table 1) $A_2 = 0.21$ and 0.24 at fields of 60 and 6000 gauss, respectively. The trend of our results is consistent with the results of Stiening and Deutsch who have reported A_2 values of 0.18 and 0.21 at

Table 5. Paramagnetic Correction Factors Given by Günther and Lindgren (45)

Experiment	Life Time in Nanoseconds	Ions in Liquid	Paramagnetic Correction Factor, β (27°C)
Sm^{153}	3.8	Eu^{+3}	0.52
Eu^{154}	1.2	Gd^{+3}	1.23
Ce^{143}	4.2	Pr^{+3}	2.00

0 and 3200 gauss, respectively. Their lower A_2 coefficients were obtained in experiments where NaI detectors were used to observe both radiations. In our experiments a Ge(Li) detector was used for the 123 keV radiation, in conjunction with a NaI detector for the 1270 keV radiation. This combination was expected to have a better resolving capability than that of Stiening and Deutsch. The lower energy portion of the coincidence spectrum, as shown in Figure 15, played an important role in our results and was subtracted from the main peak in order to obtain the true coincidences.

For the spin sequence 2(1)2(2)0 it is expected that $A_2 = 0.25$, which is in agreement with our results for a decoupling field of 6000 gauss, viz. $A_2 = 0.24 \pm 0.02$. (The notation here is $J_1(L_1)J_2(L_2)J_3$ with J_1, J_2 and J_3 the spins of the three nuclear states and L_1 and L_2 the multipole orders of the first and second radiations, respectively.)

Sb^{125} Experiments

Notwithstanding the 1.6 nanosecond lifetime of the 35.5 keV level, one does not expect an attenuation of the 427-35.5 keV cascade. Unlike the elements of the rare earth group, sources of dissolved Sb salts are not ferromagnetic and it is not expected that strong magnetic fields should be present at the nuclei. Our magnetic decoupling experiments showed no decoupling effects at fields up to 6000 gauss. It is concluded that the results and interpretations of directional correlations proceeding through the 35.5 keV level, as previously reported from this laboratory (20), are not affected by magnetic interactions in the intermediate state.

Sm^{153} Experiments

The 3.8 nanosecond lifetime of the 103 keV level of the daughter Eu^{153} nuclide suggests the possibility of attenuation of directional correlations involving this level. However, the paramagnetic correction factor, which is given to be 0.52 at 27°C for the Eu^{+3} ions, is smaller than in other rare earth elements studied here.

Our experiments have failed to show any decoupling effects at fields up to 6000 gauss. The average results of our experiments show an isotropic radiation distribution for the 70-103 keV cascade, which is consistent with the results of Sund and Wiedenbeck (27) and McGowan (28). These results are also consistent with the conclusions of Graham et al. (46) based on their studies of the L/K, L_{II}/L_I and L_{III}/L_I internal conversion coefficient ratios. They reported $|\delta| \simeq 0.14$ for both the 70 and the 103 keV transitions. The A_2 coefficients predicted for the 5/2 (1,2) 3/2 (1,2) 5/2 cascade utilizing these values for the mixing parameters δ are shown in Table 6. Of the four possible combinations, our experiments rule out case (2) where $\delta(70) = 0.14$ and $\delta(103) = -0.14$. The other three combinations are consistent with our experimental results. A plot of $A_2(70)$ versus δ for $-0.2 < \delta < 0.2$ is given in Figure (19). A similar plot for $A_2(103)$ can be obtained by replacing δ with $-\delta$.

Ce^{143} Experiments

The 4.2 nanosecond lifetime of the 57 keV level was the longest in our experiments. Pr^{+3} ions of the daughter nucleus have a paramagnetic correction factor of 2.00 at 27°C, which is larger than the

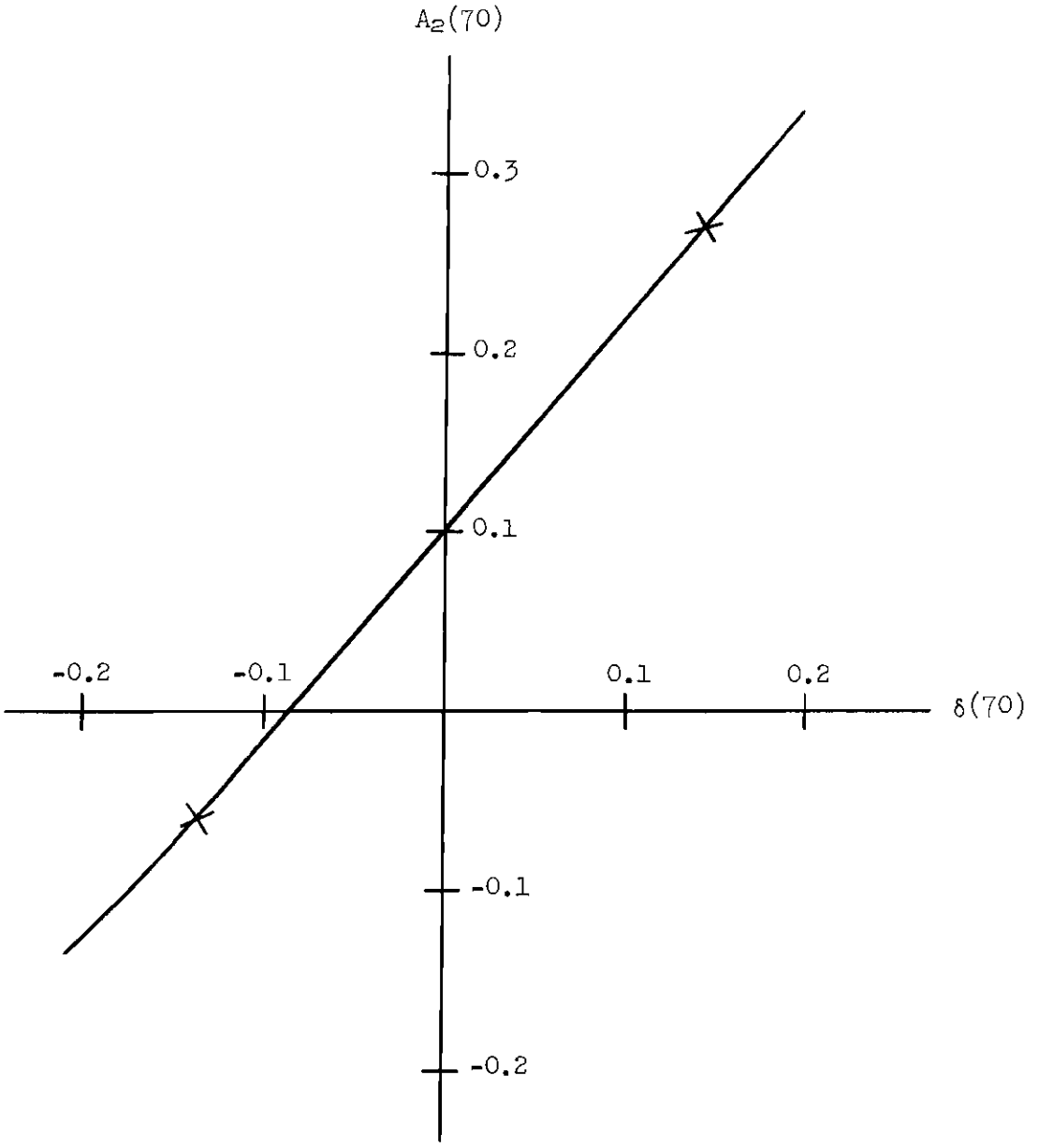

Figure 19. Plot of $A_2(70)$ Versus $\delta(70)$

Table 6. Directional Correlation Coefficients Using Mixing Parameters of Graham et al. (46)

CASE	$\delta(70)$	$A_2(70)$	$\delta(103)$	$A_2(103)$	A_2
(1)	0.14	0.27	0.14	-0.06	-0.016
(2)	0.14	0.27	-0.14	0.27	0.073
(3)	-0.14	-0.06	0.14	-0.06	0.004
(4)	-0.14	-0.06	-0.14	0.27	-0.016

factors for Eu^{+3} and Gd^{+3} ions. These facts suggest a strong possibility that the 293-57 keV directional correlations might be attenuated due to static magnetic interactions. Rotations of the radiation pattern of this cascade have been measured by Sunyar and Thieberger (35) in a 7350 gauss field. They have reported, in a private communication to Gelletly et al. (34), an A_2 value of 0.18 as a result of their experiments involving different delay times.

The present results, summarized in Table 4, indicate that the attenuation found in this case was the strongest one among our experiments. On the basis of our series of experiments, we adopt the values $A_2 = 0.18 \pm 0.02$ for the unattenuated directional correlation of the 293-57 keV cascade.

The spins of the ground states of Pr^{143} and the parent Ce^{143} have been established by atomic beam experiments to be 7/2 and 3/2, respectively (47). Gelletly et al. (34) find that both the 57 and the 293 keV transition are of mixed dipole and quadrupole character, based on measurements of L sub-shell conversion coefficients. Considering the dipole component of the 57 keV transition, spin values of 5/2, 7/2, or 9/2 can be assigned to the 57 keV level. A spin assignment of 3/2 to 11/2 for the 350 keV level is then consistent with a dipole component in the 293 keV transition.

The beta feeds to the 57 and 350 keV levels are taken to be first forbidden on the basis of the log $\underline{ft}$ values of 7.8 and 7.1, respectively (47), which restricts the spin of these levels to be $\leq 7/2$. Taking cognizance of the restrictions on the spin values and the mixed dipole-quadrupole nature of the two transitions, the following spin sequences

for the 293-57 keV cascade are possible: 7/2( )7/2( )7/2, 7/2( )5/2( ) 7/2, 5/2( )7/2( )7/2, 5/2( )5/2( )7/2, and 3/2( )5/2( )7/2.

The magnitudes of the mixing parameters for the 57 and 293 keV transitions are closely determined by the conversion coefficient work of Gelletly et al. (34) to be $|\delta|$ (57) = 0.04 and $|\delta|$ (293) = 0.75. The directional correlation result, $A_2 = 0.18 \pm 0.02$, then places additional restrictions on the properties of the cascade, as may be seen with the aid of Table 7. The table summarizes, for the reasonable choices of spin sequence, the possible theoretical directional correlation results which are consistent with the internal conversion coefficient measurements.

The spin sequence 3/2( )5/2( )7/2 with $\delta(293) = -0.75$ and $\delta(57) = -0.04$ is consistent with the experimental data. Also consistent with the data is the sequence 7/2( )5/2( )7/2 with $\delta(293) = 0.75$ and $\delta(57) = -0.04$. Systematic errors usually tend to result in the observation of a too small value for the magnitude of the directional correlation coefficient. Furthermore, it is possible that even the largest magnetic field used in the present experiments did not quite restore the correlation to the unattenuated value. Hence, the data should be construed as not definitely ruling out the sequence 7/2( )7/2 ( )7/2 with $\delta(293) = 0.75$ and $\delta(57) = 0.04$.

A spin assignment of 7/2 for the 57 and 350 keV levels requires that the corresponding beta feeds be first forbidden unique. It is usually expected that the unique transitions have larger log ft values (48) than those of 7.8 and 7.1, as reported by Chiao and Raman (47). Narasimha Raju et al. (49) have measured the beta-gamma directional

Table 7. Computation of Directional Correlation Coefficients

J_1	$\delta(293)$	$A_2(293)$	J_2	$\delta(57)$	$A_2(57)$	A_2
7/2	0.75	-0.55	7/2	0.04	-0.40	0.22
	0.75	-0.55		-0.04	-0.47	0.26
	-0.75	0.17		0.04	-0.40	-0.07
	-0.75	0.17		-0.04	-0.47	-0.08
7/2	0.75	0.87	5/2	0.04	0.08	0.07
	0.75	0.87		-0.04	0.19	0.16
	-0.75	-0.46		0.04	0.08	-0.04
	-0.75	-0.46		-0.04	0.19	-0.09
5/2	0.75	-0.73	7/2	0.04	-0.40	0.29
	0.75	-0.73		-0.04	-0.47	0.34
	-0.75	1.09		0.04	-0.40	-0.44
	-0.75	1.09		-0.04	-0.47	-0.51
5/2	0.75	-0.69	5/2	0.04	0.08	-0.05
	0.75	-0.69		-0.04	0.19	-0.13
	-0.75	0.28		0.04	0.08	0.02
	-0.75	0.28		-0.04	0.19	0.05
3/2	0.75	-0.74	5/2	0.04	0.08	-0.06
	0.75	-0.74		-0.04	0.19	-0.14
	-0.75	1.08		0.04	0.08	0.08
	-0.75	1.08		-0.04	0.19	0.20

correlation between the beta group feeding the 350 keV level and the 293 keV gamma and found it to be nearly isotropic. The theoretical partial directional correlation coefficient for the first borbidden unique beta transition in this case is $A_2(\beta) = -0.65$. The theoretical partial gamma directional correlation coefficient for the mixing parameter $|\delta| = 0.75$ is 1.09 or -0.73 (depending on the sign of δ) for the 7/2( )5/2( )7/2 sequence and 0.17 or -0.55 for the 7/2( )7/2( )7/2 sequence. Since the absolute value of the product of these coefficients is then $|A_2(\beta)\ A_2(293)| \geq 0.11$, it is concluded that the beta feed to the 350 keV level is not a unique transition.

It is concluded that the proper spin assignment for the 350 keV level is 3/2.

CHAPTER V

SUGGESTIONS FOR FUTURE RESEARCH

Study of the attenuation of directional correlations caused by static magnetic fields might resolve a number of discrepancies in the assignment of spin quantum numbers. It is possible that evaluation of previously unobserved attenuations in some instances could reconcile the results of gamma-gamma directional correlation experiments with those of other types of experiments. This experimental technique should be used whenever a question of this type arises.

The paramagnetic correction factors given by Günther and Lindgren (45) indicate that in Ho^{+3}, Er^{+3} and Dy^{+3} ions, much stronger static magnetic fields will prevail at the corresponding nuclei than the ones encountered in our work. The relationship between the attenuation and the paramagnetic correction factors is certainly interesting and should be further investigated in the decay of ${}_{65}Tb^{160}$ into ${}_{66}Dy^{160}$, which proceeds through a 2 nanosecond level and in the decay of ${}_{67}Ho^{166}$ into ${}_{68}Er^{166}$, which proceeds through a 1.8 nanosecond level. Er^{+3} and Dy^{+3} ions have β factors of 6.82 and 6.02 at 27°C, respectively, and the directional correlations involving these levels may be more strongly attenuated than in the case of the Ce^{143} decay.

On the theoretical side there is need for development of a formula which relates the static magnetic interactions to the attenuation of the directional correlation coefficients.

APPENDIX A

SUMMARY OF THE PERTURBED DIRECTIONAL CORRELATIONS FORMALISM

This Appendix is intended to summarize only the pertinent aspects of the perturbed directional correlations theory related to this thesis work. For a complete treatment of the theory the reader should refer to the articles by Alder (11), Abragam and Pound (12) and Steffen (5). The theory presented here is essentially a summary of the article by Fraunfelder and Steffen (13).

The first part of this Appendix gives a short derivation of the perturbed directional correlation function from the unperturbed correlation function. An attempt has been made to point out the physics involved in the presence of a perturbing mechanism which influences the correlation function.

The second part which deals with static magnetic fields is intended to summarize the mathematics involved in the two topics discussed qualitatively in the introductory chapter, namely, the claims that any axially symmetric static magnetic field which is applied parallel to the direction of one of the radiations does not alter the directional correlation and the possibility of obtaining the unperturbed correlation function by breaking the coupling between the nucleus and the electron shell by the application of a strong magnetic field.

Perturbed Directional Correlation Function

The unperturbed directional correlation function is given by (13)

$$W(\bar{R}_1,\bar{R}_2) = S_1 S_2 \sum_{\substack{m_f\ m \\ m_i\ m'}} < m_f|\vec{H}_2|m > < m|\vec{H}_1|m_i> < m'|\vec{H}_1|m_i>^* < m_f|\vec{H}_2|m'>^* \quad (A.1)$$

where the symbols S_1, S_2 indicate summations over all unmeasured radiation properties, such as the polarizations for the first and second radiations, respectively. The summation is performed over the initial (m_i), intermediate (m,m') and the final (m_f) states. The interaction of the nucleus with the radiation field is described by the interaction operators $\vec{H}_1$ and $\vec{H}_2$.

One can rewrite Equation (A.1) as

$$W(\bar{R}_1,\bar{R}_2) = S_1 S_2 \sum_{\substack{m_i\ m_a\ m_b \\ m_f\ m'_a\ m'_b}} < m_f|\vec{H}_2|m_b > < m_a|\vec{H}_1|m_i> \delta_{m_a m_b} < m_f|\vec{H}_2|m'_b >^* \quad (A.2)$$

$$X < m'_a|\vec{H}_1|m_i >^* \delta_{m'_a m'_b}$$

when the intermediate level is under the influence of an extranuclear field. Clearly, in the presence of a perturbation, the intermediate states $|m_a>$ and $|m'_a>$ after the emission of the first radiation are different from $|m_b>$ and $|m'_b>$ which describe these intermediate states just before the emission of the second radiation. When the perturbation is removed, then the states $|m_a>$ and $|m'_a>$ after the emission of the first radiation, are identical with the initial states $|m_b>$ and $|m'_b>$

of the second radiation. If we let $\vec{K}$ represent the perturbation operator which acts on the intermediate state during the time interval t between the emission of two successive radiations, then we can also represent the changing of the $|m_a>$ states into the $|m_b>$ states by a unitary operator $\Lambda(t)$. This time evolution operator $\Lambda(t)$ satisfies the Schrödinger equation

$$\frac{\partial}{\partial t} \Lambda(t) = - (2\pi i/h)\vec{K} \Lambda(t), \tag{A.3}$$

and for static interactions, where the perturbing Hamiltonian $\vec{K}$ is independent of time, the solution of Equation (A.3) is simply

$$\Lambda(t) = \exp(-2\pi i\vec{K}t/h). \tag{A.4}$$

The state vector $\Lambda(t)|m_a>$ can be expressed in terms of $|m>$ vectors which form a complete set in the following manner:

$$\Lambda(t)|m_a> = \sum_{m_b} |m_b> < m_b|\Lambda(t)|m_a> . \tag{A.5}$$

Similarly,

$$\Lambda(t)|m_a'> = \sum_{m_b'} |m_b'> < m_b'|\Lambda(t)|m_a'> . \tag{A.6}$$

Using the time evolution operator $\Lambda(t)$ we rewrite Equation (A.2)

$$W(\bar{R}_1,\bar{R}_2) = S_1S_2 \sum_{\substack{m_i\ m_a \\ m_f\ m_a'}} < m_f|\vec{H}_2\Lambda(t)|m_a> < m_a|\vec{H}_1|m_i> \ X \tag{A.7}$$

$$X < m_f|\vec{H}_2|\Lambda(t)|m_a'>^* < m_a'|\vec{H}_1|m_i>^*$$

substituting Equations (A.5) and (A.6) into (A.7) we obtain,

$$W(\bar{R}_1,\bar{R}_2) = S_1S_2 \sum_{\substack{m_i\ m_a\ m_a' \\ m_f\ m_b\ m_b'}} < m_f|\vec{H}_2|m_b> < m_b|\Lambda(t)|m_a> \qquad (A.8)$$

$$X < m_a|\vec{H}_1|m_i> < m_f|\vec{H}_2|m_b'>^* < m_b'|\Lambda(t)|m_a'> < m_a'|\vec{H}_1|m_i>^*.$$

Comparing Equations (A.2) and (A.8) one can associate the matrix elements $< m_b|\Lambda(t)|m_a> < m_b'|\Lambda(t)|m_a'>^*$ with the extranuclear perturbation.

If one restricts the problem only to directional correlations and to circular polarization correlations, after various manipulations, one obtains (4) an expression for the time differential perturbed directional correlation function in the form

$$W(\bar{R}_1,\bar{R}_2,t) = \sum_{k_1\ k_2\ N_1\ N_2} A_{k_1}^{(1)}\ A_{k_2}^{(2)}\ G_{k_1\ k_2}^{N_1\ N_2}(t)\left[(2k_1+1)(2k_2+1)\right]^{-1/2} \qquad (A.9)$$

$$X\ Y_{k_1}^{N_1^*}(\theta_1,\varphi_1)Y_{k_2}^{N_2}(\theta_2,\varphi_2)$$

where the second radiation is observed within the time t to t+dt after the emission of the first radiation. In this formula the Y_k^N are ordinary spherical harmonics and the indices k_1 and k_2 are even integers which obey the inequalities:

$$0 \le k_1 \le 2I \qquad 0 \le k_2 \le 2I$$

$$0 \le k_2 \le 2L_1 \qquad 0 \le k_2 \le 2L_2$$

where L_1 and L_2 are the higher orders in the multipole expansions of the first and second radiations, respectively. I is the spin of the intermediate state. The relationship between the directions of the radiations and the angles of the spherical harmonics, are shown in Figure 20 . The coefficients $A_k^{(1)}$ and $A_k^{(2)}$ are determined by the spin values of the nuclear cascade and the multipolarities of the consecutive gamma rays. Ferentz and Rosenweig (4) express these partial angular correlation coefficients in terms of the mixing parameters δ and the F_k coefficients they have tabulated. Rose and Brink (6) give the A_k coefficients in terms of their R_k coefficients where a phase-consistent approach was followed in their derivation. The phase relationship between the F_k and R_k coefficients is given by Salzberg (19).

Alder (3) has shown that for axially symmetric fields the perturbation factor becomes:

$$G^{N\ N}_{k_1\ k_2}(t) = \sum_{m_a\ m_b} (-1)^{2I + m_a + m_b} \left[(2k_1+1)(2k_2+1)\right]^{1/2} \qquad (A.10)$$

$$\begin{Bmatrix} I & I & k_1 \\ m_a' & -m_a & N_1 \end{Bmatrix} \begin{Bmatrix} I & I & k_2 \\ m_b' & -m_b & N_2 \end{Bmatrix} \langle m_b|\Lambda(t)|m_a\rangle^* \langle m_b'|\Lambda(t)|m_a'\rangle^*$$

whenever the projection of the nuclear spin operator $\vec{I}$ on the Z-axis is a good quantum number, or, in other words, whenever $\vec{I}_Z$ commutes with the perturbing Hamiltonian $\vec{K}$.

In order to obtain the unperturbed correlation function, one essentially turns off the perturbation by letting t=0 such that the unitary evolution operator $\Lambda(t) = \exp[-i\hbar\vec{K}(t)/2\pi]$ becomes unity. Then

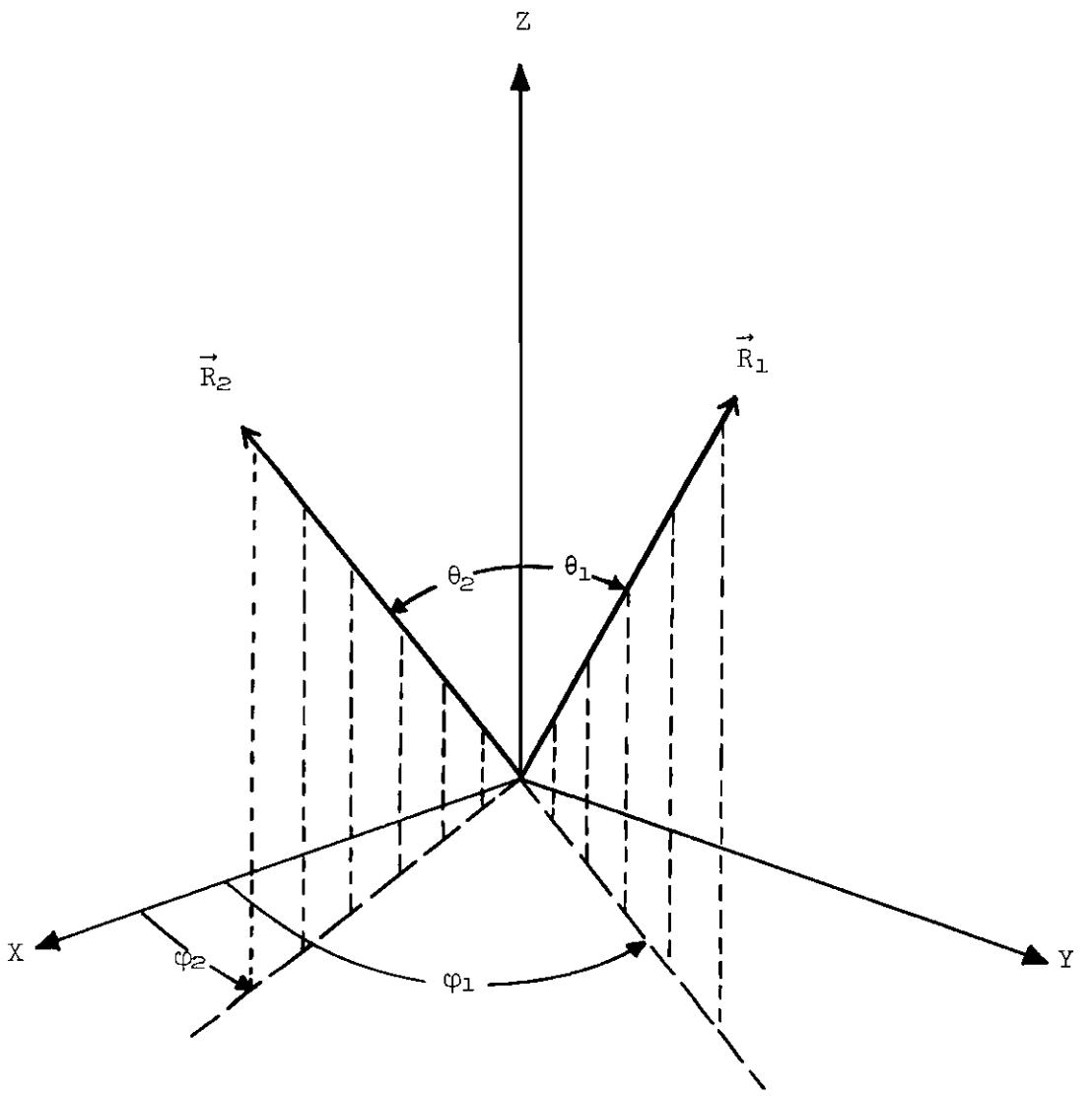

Figure 20. Angular Coordinates of the Propagation Directions $\vec{R}_1$ and $\vec{R}_2$

$$G^{N_1\ N_2}_{k_1\ k_2}\ (t = 0) = \delta_{k_1 k_2}\ \delta_{N_1 N_2}$$

and we obtain the unperturbed correlation function

$$W(\theta,0) = \frac{1}{4\pi} \sum_k A_k^{(1)}\ A_k^{(2)}\ P_k(\cos\theta). \tag{A.11}$$

In an actual experiment where the coincidence circuitry has a delay time T and a resolving time τ_o the measured correlation function is

$$\overline{W(\bar{R}_1,\bar{R}_2,T-\tau_o,T+\tau_o)} = \frac{\int_{T-\tau_o}^{T+\tau_o} e^{-t/\tau}\ W(k_1,k_2,t)\ dt}{\int_{T-\tau_o}^{T+\tau_o} e^{-t/\tau}\ dt} \tag{A.12}$$

where τ is the mean life of the intermediate level. The limits of integration take into account the fact that the second radiation is accepted within a finite time interval, $T-\tau_o$ to $T+\tau_o$, after the first radiation has been emitted.

The time integrated perturbation factor is given by

$$G^{N_1\ N_2}_{k_1\ k_2}\ (T-\tau_o,T+\tau_o) = \frac{\int_{T-\tau_o}^{T+\tau_o} e^{-t/\tau}\ G^{N_1\ N_2}_{k_1\ k_2}\ dt}{\int_{T-\tau_o}^{T+\tau_o} e^{-t/\tau}\ dt}\ . \tag{A.13}$$

Static Magnetic Fields

If the perturbation is due to the interaction of the magnetic moment of the nucleus with the external magnetic field, the matrix elements of the evolution operator $\Lambda(t)$ can be expressed in the m-representation. Taking a unitary operator which diagonalizes the

interaction Hamiltonian $\vec{K}$

$$U\vec{K}U^{-1} = E$$

where E are the energy eigenvalues of the diagonal energy matrix E, one can rewrite the evolution operator as

$$\Lambda(t) = U^{-1}e^{-i2\pi Et/h}\,U$$

using the relationship

$$Ue^{-i2\pi\vec{K}t/h}\,U^{-1} = e^{-i2\pi Et/h}\ .$$

One can rewrite the matrix elements of $\Lambda(t)$ in terms of the matrix elements $< m|n >$ of the unitary matrix U as

$$< m_b|\Lambda(t)|m_a> = \sum_n < n|m_b>^* e^{-i2\pi E_n t/h} < n|m_a> . \qquad (A.14)$$

For a pure, axially symmetric magnetic field, the symmetry axis of the interaction can be chosen parallel to the Z axis, which means that the projection of the nuclear spin on this axis is a good quantum number. In other words, the operator $\vec{I}_Z$ commutes with the perturbing Hamiltonian $\vec{K}$. One can then rewrite Equation (A.14) in terms of the eigenfunctions $|m >$ as:

$$< m_b|\Lambda(t)|m_a> = e^{-i2\pi E_m t/h}\ \delta_{m\,m_a}\delta_{m\,m_b}$$

and the perturbation factor in Equation (A.10) becomes

$$G^{N\ N}_{k_1\ k_2}(t) = \sum_m \left[(2k_1+1)(2k_2+1)\right]^{1/2} \begin{Bmatrix} I & I & k_1 \\ m'-m & N & \end{Bmatrix} \begin{Bmatrix} I & I & k_2 \\ m'-m & N & \end{Bmatrix} \quad (A.15)$$

$$X\ e^{-i2\pi(E_m - E_{m'})t/h} .$$

Now if we consider the case of a static magnetic field which has its symmetry axis parallel to the direction of one of the radiations, for example R_1, we obtain

$$G^{N\ N}_{k_1\ k_2}(t) = \delta_{k_1\ k_2}\delta_{N_1\ N_2}$$

since $m = m'$ and $E_m - E_{m'} = 0$.

Then substituting this in Equation (A.9) one can obtain

$$W(\bar{R}_1,\bar{R}_2,t) = \frac{1}{4\pi} \sum_k A_k^{(1)}\ A_k^{(2)}\ P_k(\cos\theta)$$

which is just the unperturbed correlation function. As it has been pointed out in the introduction, any static magnetic field which is applied parallel to the direction of one of the radiations does not alter the angular correlation. Semiclassically this means that the angular momentum of the nucleus in the intermediate state is precessing around the field axis and the projections of the angular momentum along this axis are not changing. Quantum mechanically, this is equivalent to saying that the populations of the m levels along the axis of symmetry remain the same.

By the same token, one can see how the unperturbed correlation function may be obtained by breaking the I-J coupling in a free atom.

A strong magnetic field will decouple the interaction between the angular momentum J of the electron shell and the angular momentum I of the nucleus. Semiclassically, this means that the vectors $\bar{I}$ and $\bar{J}$ are now independently precessing around the field axis (see Figure 5). In the quantum mechanical language, we say that the projections of $\bar{I}$ and $\bar{J}$, along the quantization axis, which are m and M respectively, are good quantum numbers. In other words, the interaction Hamiltonian $\vec{K}$ is diagonal in the m and M representation.

The mean I-J coupling energy in a strong magnetic field is

$$E_{I-J} = a\ m\ M$$

where a is the magnetic hyperfine structure constant defined by

$$a = \frac{\mu}{I} X \frac{\overline{H(0)}}{J} \ .$$

$\overline{H(0)}$ is the magnetic field produced at the nucleus by the electron shell. Since the energy of a magnetic dipole in a magnetic field is

$$E_d = - \frac{\mu\ B_o}{I}\ m$$

the energy levels of the nucleus in the intermediate state are given by

$$E_n = a\ m\ M - \frac{\mu\ B_o}{I}\ m \ .$$

Then the perturbation factor in Equation (A.10) is simply

$$G^{N\ \ N}_{k_1\ k_2}(t) = \frac{1}{2J+1} \sum_{-J}^{+J} \sum_{m} \left[(2k_1+1)(2k_2+1)\right]^{1/2} \begin{Bmatrix} I & I & k_1 \\ m' & -m & N \end{Bmatrix} X \quad \text{(A.16)}$$

$$X \quad \begin{Bmatrix} I & I & k_2 \\ m' & -m & N \end{Bmatrix} e^{-i2\pi(aM - \frac{\mu B_o}{I})Nt/h}$$

where a summation over the electronic states has been performed, taking into account the (2J+1) fold degeneracy. Performing the summation over m, one obtains

$$G^{N\,N}(t) = \frac{e^{-iN\omega t}}{2J+1} \quad X \quad \frac{\sin[(\pi aN/h)(2J+1)t]}{\sin[(\pi aN/h)t]}$$

which is independent of k. If we again choose the direction of the magnetic field $\vec{B}$ parallel to $\vec{R}_1$, we have

$$Y_k^N(0,\varphi_1) = [(2k+1)/4\pi]^{1/2} \delta_{N\,0},$$

$$Y_k^0(\theta_2,\varphi_2) = [(2k+1)/4\pi]^{1/2} P_k(\cos\theta_2) .$$

Substituting these expressions into Equation (A.9), one obtains the unperturbed correlation function.

APPENDIX B

ANALYSIS OF EXPERIMENTAL DATA AND CORRECTIONS

In order to investigate the effect of an external magnetic field, the A_2 directional correlation coefficient for the cascade under consideration was first measured without an external field and then with the field turned on. Then, these values were compared to see if indeed any decoupling occurred.

The theoretical expression for the A_2 coefficients involving data which were collected at 90°, 180° and 270° positions is given by

$$A_2 = \frac{F_{180} - 1}{1 + \frac{1}{2} F_{180}} \tag{B.1}$$

$$F_{180} = \frac{N_{180} - N_{ACC}}{\frac{1}{2}(N_{90} + N_{270}) - N_{ACC}} \, . \tag{B.2}$$

N_{180} is the normalized rate of coincidences at 180° and N_{ACC} is the normalized rate of accidental coincidences. The expression $N_{180} - N_{ACC}$ therefore gives the number of true coincidences at 180°. The denominator of Equation (B.2) gives the normalized rate of true coincidences at either 90° or 270° since N_{90} and N_{270}, which correspond to the number of total coincidences at 90° and 270° respectively, should be identical from the theoretical point of view. The expression labeled A_2 here is equal to the A_2 coefficient only if the A_4 coefficient is zero. However, the

expression given here is a valid index for comparison with and without the magnetic field in any event.

In the measurement of A_2 for a given cascade one of the main points of concern was the possibility of unwanted radiations being present when a NaI(Tℓ) detector was employed in one channel. This problem was handled using the Ge(Li) detectors, which had better energy resolving capabilities, to investigate the spectral region of interest. The unwanted portions of the spectrum were blocked out as much as possible by adjustment of single channel pulse height analyzer in the NaI(Tℓ) channel.

The source centering procedure introduced another problem which was handled in the following way. The number of singles counts registered in the movable counter varied as much as 1.5% from one position to another. The coincidence rate at a given angle was therefore divided by the corresponding singles rate in the movable counter in order to compensate for such variations. This quantity, which was the coincidence rate divided by the singles rate in the movable counter, will be referred to as the normalized coincidence rate.

The part of the computer program which dealt with preliminary data reduction and analysis printed out the average normalized coincidence rate at each angle, where the data collected at a given angle was averaged over the total number of runs at that particular position. This information could either be printed out over a range of about 64 channels or be subjected to immediate curve fitting analysis as was mentioned in Chapter II.

The Least Squares Fit Programs

The data displayed on the scope could be analyzed using either of the programs named FIT1 or FITO. Both of these programs were designed to calculate the area under a given peak using 1 to 5 Gaussian peaks and a linear background. In this way the contributions to the background from other parts of the spectrum were subtracted so that the actual normalized coincidence rate for the desired cascade was obtained.

A brief discussion of these programs will be given below. For a complete discussion of these programs the reader should refer to Bevington (50) and Salzberg (44).

The object of representing the N data points y_i by a suitable function

$$y(x_i) = a_1 - a_2 x_i + a_3 \exp\left[-\frac{1}{2}\left\{\frac{x_i - a_4}{a_5}\right\}^2\right] + a_6 \exp\left[-\frac{1}{2}\left\{\frac{x_i - a_7}{a_8}\right\}^2\right] + \cdots \tag{B.3}$$

was accomplished by minimizing the expression

$$X^2 = \sum_{i=1}^{N} [\, y_i - y(x_i) \,]^2 \tag{B.4}$$

which is referred to as "deviation." Two methods were used to determine the values of the parameters a_j of the function $y(x_i)$ which gave a minimum of X^2.

One method was called the grid search method (50) and FIT program

was designed to accomplish this. The grid search method was suitable if the variation of X^2 with each parameter a_j was fairly independent of how well other parameters were optimized. It involved optimizing a parameter a_j independently so that after successive iterations a local minimum could be approached. This parameter a_j was incremented by a determined amount δa_j such that X^2 started decreasing. This incrementation was continued until an increase in X^2 was to be observed. A parabolic interpolation was made to determine the minimum of X^2 for the parameter a_j. Then X^2 was minimized for each parameter in turn. This procedure was repeated until the last iteration yielded a negligible decrease in X^2. In this way an absolute minimum was found. One disadvantage of this method was its slowness in converging towards a minimum. However, the scope display facility was of considerable help here in reducing the calculation time. The initial parameters were suitably chosen such that the function $y(x_i)$ and the original data points were matched visually as closely as possible.

The second program named FITO was considerably faster than the FIT program since it utilized a combination of grid search and parabolic extrapolation methods. FITO program started with a grid search method and when it reached a point where two successive deviations differed by less than 20% it started executing a different method. In this method the function X^2 was expanded using an analytical expression for the variation of X^2. The first order Taylor's series expansion for the function X^2 in terms of the parameters a_j were given by

$$X^2 = X_0^2 + \sum_{j=1}^{n} \frac{\partial X_0^2}{\partial a_j} \delta a_j \qquad (B.5)$$

where X_0^2 was the starting point value for X^2 and δa_j were the increments in the parameter a_j.

The least squares method gave the optimum values for the increments δa_j at a point in parameter space where the function X^2 was at a minimum. In other words,

$$\frac{\partial X^2}{\partial a_k} = \frac{\partial X_0^2}{\partial a_k} + \sum_{j=1}^{n} \left(\frac{\partial X_0^2}{\partial a_j \partial a_k} \delta a_j \right) = 0 \qquad (B.6)$$

For n such parameters the resulting n simultaneous linear equations in δa_j were solved. This least squares method of expanding X^2 to the first order in a Taylor Series was essentially a parabolic extrapolation of X^2 (50). The parabolic approximation was accurate when the starting point was close to a minimum. This problem has been handled in our experiments by the scope display facility.

Accidental Coincidences

The accidental coincidence rates were collected separately at three different positions, namely 90°, 180° and 270° to check if this rate varied with respect to the position. No such variation was found. The same rate was also compared with the magnetic field off and on at about 6000 gauss. Again no variation was found.

Finite Solid Angle Corrections

The angular correlation function

$$W(\theta) = \sum_{k=0}^{k_{max}} A_k P_k (\cos\theta) \qquad (B.7)$$

is applicable to the idealized case where the two detectors are considered as two points. The finite size of the detectors in an actual experiment necessitates the use of correction factor defined according to

$$A_i\ (\text{corr}) = \frac{A_i(\text{exp})}{Q_i(1)\ Q_i(2)} \qquad (B.8)$$

where $A_i(\text{corr})$ is the directional correlation coefficient after geometrical corrections, $A_i(\text{exp})$ is the experimental value of this coefficient and the $Q_i(1)$ and the $Q_i(2)$ are the correction factors for the first and the second detectors, respectively. These correction factors (4, 13) depend on the energy of the gamma rays, the size of the detector and the distance between the source and the detector. The correction factors for Ge(Li) detectors have recently appeared in the literature and our calculations are based on the article by Camp and Van Lehn (51). Similar correction factors have been used for Si(Li) (52) and NaI (13) detectors. Table 8 shows the correction factors used in our experiments.

Analysis Of Sb^{125} Experiment

The computer print out of the coincidence rates were analyzed over a range of 25 channels (see Table 9). In order to calculate the area below the main coincidence peak, a least squares fit was made using a Gaussian peak and a linear background (see equation B.3). Inclusion of this linear background, of the form $a_1 - a_2x$ was intended to correct for background radiations, scattering, etc. Final para-

Table 8. Geometrical Correction Factors

EXPERIMENTS	Eu^{154}		Sb^{125}		Sm^{153}		Ce^{143}	
Detector	Ge(Li) LGC 3.5X	NaI	Si(Li)	NaI	Ge(Li) LGC 3.5X	Ge(Li) Ortec	Ge(Li) LGC 3.5X	NaI
Gamma Ray Energy (keV)	123	1270	35.5	427	70	103	57	293
Source to Crystal Distance (cm)	7.0	10.2	5.9	9.7	8	6.5	7.0	8.5
Frontal Active Area of Crystal (mm^2)	905	4558	30	4558	905	892	905	4558
A_2 Correction Factor for Each Detector	0.961	0.938	0.998	0.931	0.970	0.955	0.957	0.888
Product of A_2 Correction Factors	0.901		0.929		0.932		0.850	

Table 9. Data for the 427-35.5 keV Cascade in Sb^{125} at 6000 Gauss.

CHANNEL	NORMALIZED COINCIDENCE RATES PRINTED BY COMPUTER			
	90°	180°	270°	Accidentals
1	24	26	37	9
2	38	29	33	9
3	36	24	28	12
4	29	32	32	10
5	34	30	29	12
6	39	30	33	14
7	39	31	38	14
8	36	39	44	18
9	42	52	45	20
10	112	107	92	39
11	272	312	272	102
12	614	703	599	193
13	762	1000	758	257
14	553	729	560	186
15	249	335	259	71
16	62	93	75	24
17	21	24	21	9
18	12	11	6	4
19	4	7	7	2
20	7	7	8	6
21	7	9	4	4
22	5	7	7	6
23	8	7	7	6
24	8	8	9	5
25	2	7	6	7

meters which were used to calculate the area under the coincidence peak are given in Table 10 in addition to other pertinent information.

The symmetry in this experiment was reasonably good since the areas at 90° and 270° differ at most by less than 2%. The ratio of true coincidences at 180° to accidental coincidences was about 2.7 to 1.

Table 10. Parameters Used in FITO to Calculate the Coincidence Rates for the Data in Table 9

Angle	a_1	a_2	a_3	a_4	a_5	Coinc. Rate
90°	48.30	1.82	366	12.93	1.34	1228
180°	33.58	1.13	451	13.03	1.31	1480
270°	47.47	1.77	371	12.96	1.35	1254
Acc.	47.48	1.25	121	12.91	1.33	402

BIBLIOGRAPHY

1. D. R. Hamilton, Physical Review, 58, 122 (1940).

2. E. Sagre, ed., Experimental Nuclear Physics, 3, 373 (1955).

3. H. Fraunfelder, Annual Review of Nuclear Science, 2, 129 (1953).

4. K. Siegbahn, ed., Alpha-Beta-and Gamma-Ray Spectroscopy, North Holland Publishing Company, Amsterdam, (1966).

5. R. M. Steffen, Advances in Physics, 15, 293 (1955).

6. H. J. Rose and D. M. Brink, Reviews of Modern Physics, 37, 306 (1967).

7. L. C. Biedenharn and M. E. Rose, Reviews of Modern Physics, 25, 729 (1953).

8. E. L. Brady and M. Deutsch, Physical Review, 72, 870 (1947).

9. R. Stiening and M. Deutsch, Physical Review, 121, 1484 (1961).

10. G. Goertzel, Physical Review, 70, 897 (1946).

11. K. Alder, Physical Review, 84, 369 (1951).

12. A. Abragam and R. V. Pound, Physical Review, 92, 943 (1953).

13. H. Fraunfelder and R. M. Steffen, edited by E. Karlsson, E. Matthias and K. Siegbahn, Perturbed Angular Correlations, North Holland Publishing Company, Amsterdam, (1964).

14. N. J. Stone, R. B. Frankel and D. A. Shirley, Physical Review, 172, 1243 (1968).

15. T. Inamura, J. Phys. Soc. Japan, 24, 1 (1968).

16. A. Marelius, J. Lindskog, Z. Awwad, K. C. Valivaara, S. E. Hagglund, and J. Pihl, Nuclear Physics, A148, 433 (1970).

17. J. S. Geiger, R. L. Graham, J. Bergstrom and F. Brown, Nuclear Physics, 68, 352 (1965).

18. E. P. Mazets and Y. V. Sergeenkov, Bull. Acad.Sci. USSR, Phys. Ser. 30, 1237 (1966).

19. J. B. Salzberg, Ph.D. Thesis, Georgia Institute of Technology, July, 1971.

20. L. D. Wyly, J. B. Salzberg, E. T. Patronis, Jr., N. S. Kendrick and C. H. Braden, Physical Review, C3, 2442 (1971).

21. J. Ungrin and M. W. Johns, Nuclear Physics, A127, 353 (1969).

22. M. Vergnes and N. Marty, J. Physics Radium, 17, 908 (1958).

23. F. K. McGowan, Physical Review, 93, 163 (1954).

24. T. D. Nainan, Physical Review, 123, 1751 (1961).

25. V. S. Dubey, C. E. Mandeville and M. A. Rothman, Physical Review, 103, 1430 (1956).

26. R. L. Graham, G. T. Ewan and J. S. Geiger, Bull. Am. Phys. Soc., 5, 21 (1960).

27. R. E. Sund and M. L. Wiedenbeck, Physical Review, 120, 1792 (1960).

28. F. K. McGowan, Physical Review, 93, 163 (1954).

29. D. W. Martin, M. K. Brice, J. M. Cork and S. B. Burson, Physical Review, 101, 182 (1956).

30. G. N. Rao and H. S. Hans, Nuclear Physics, 41, 511 (1963).

31. B. Budick, I. Maleh and R. Marrus, Physical Review, 135, B1281 (1964).

32. M. A. Ludington, D. E. Raeside, J. J. Reidy and M. L. Wiedenbeck, Physical Review, 4, 647 (1971).

33. R. L. Graham, J. M. Hollander and P. Kleinheinz, Nuclear Physics, 49, 641 (1963).

34. W. Gelletly, J. S. Geiger and R. L. Graham, Physical Review, 168, 1336 (1968).

35. A. W. Sunyar and P. Thieberger, Bull. Am. Phys. Soc., 11, 407 (1966).

36. L. Simons, A. Anttila and S. Bergström, Soc. Sci. Fennica, Commentationes Phys.-Math., 30, No. 3 (1964).

37. R. V. Mancuso, J. P. Roalsvig and R. G. Arns, Physical Review, 140, B525 (1965).

38. K. P. Gopinathan, Physical Review, 139, B1467 (1965).

39. E. Bozek, A. Z. Hrynkiewicz, S. Ogaza, M. Rvbicka and J. Styczen, Physics Letters, 6, 89 (1963).

40. R. M. Levy, Ph.D. Thesis, Lawrence Radiation Laboratory Report, No. UCRL - 11663,(1964).

41. N. S. Kendrick, Foreground/Background/8 Now, Decus Proceedings, Fall, 1969.

42. C. H. Braden, Private Communication.

43. N. S. Kendrick, Private Communication.

44. J. B. Salzberg, FIT, FITO and FIT1 Programs, Georgia Institute of Technology (unpublished).

45. C. Günther and I. Lindgren, Paramagnetic Effects, Perturbed Angular Correlations, North Holland Publishing Company, Amsterdam, (1964).

46. R. L. Graham, G. T. Ewan and J. S. Geiger, Private Communication; in Nuclear Data Sheets, compiled by K. Way et al. (Printing and Publishing Office, National Academy of Sciences - National Research Council, Washington 25, D.C.)., NRC 5-5-33 and 5-5-34.

47. L. W. Chiao and S. Raman, Nuclear Data B2-1-25 (1967).

48. H. Paul, Nuclear Data, A2, 281 (1966).

49. M. L. Narasimha Raju, D. L. Sastry and E. Kondaiah, Il Nuovo Cimento, 56B, 29 (1968).

50. P. R. Bevington, Data Reduction and Error Analysis for Physical Sciences, McGraw Hill Company, New York,(1969).

51. D. C. Camp and A. L. Van Lehn, Nuclear Instruments and Methods, 76, 192 (1969).

52. R. E. Wood, P. Venugopala Rao, O. H. Puckett and J. M. Palms, Nuclear Instruments and Methods, 94, 245 (1971).

VITA

Mustafa Rauf Sarper, son of Hikmet Rauf Sarper and Fatma Mefharet Sarper, was born in Istanbul, Turkey on June 27, 1943. He attended Robert Academy in Istanbul, from which he graduated in June, 1962. He entered Georgia Institute of Technology in September 1963 and received the degrees of Bachelor of Science in Physics in June 1968 and Master of Science in Physics in June 1969.

He is married to Brenda Fraser of Kent, England.